Quasiparticle transport and g factor anisotropy

in

quantum dots

Inauguraldissertation

zur

Erlangung der Würde eines Doktors der Philosophie

vorgelegt der

Philosophisch-Naturwissenschaftlichen Fakultät

der Universität Basel

von

Robert Manfred Zielke

aus Lörrach, Deutschland

Basel, 2014

creative commons

Namensnennung-Keine kommerzielle Nutzung-Keine Bearbeitung 3.0 Schweiz
(CC BY-NC-ND 3.0 CH)

Sie dürfen: **Teilen** — den Inhalt kopieren, verbreiten und zugänglich machen

Unter den folgenden Bedingungen:

Namensnennung — Sie müssen den Namen des Autors/Rechteinhabers in der von ihm festgelegten Weise nennen.

Keine kommerzielle Nutzung — Sie dürfen diesen Inhalt nicht für kommerzielle Zwecke nutzen.

Keine Bearbeitung erlaubt — Sie dürfen diesen Inhalt nicht bearbeiten, abwandeln oder in anderer Weise verändern.

Wobei gilt:

- **Verzichtserklärung —** Jede der vorgenannten Bedingungen kann **aufgehoben** werden, sofern Sie die ausdrückliche Einwilligung des Rechteinhabers dazu erhalten.

- **Public Domain (gemeinfreie oder nicht-schützbare Inhalte) —** Soweit das Werk, der Inhalt oder irgendein Teil davon zur Public Domain der jeweiligen Rechtsordnung gehört, wird dieser Status von der Lizenz in keiner Weise berührt.

- **Sonstige Rechte —** Die Lizenz hat keinerlei Einfluss auf die folgenden Rechte:

  o Die Rechte, die jedermann wegen der Schranken des Urheberrechts oder aufgrund gesetzlicher Erlaubnisse zustehen (in einigen Ländern als grundsätzliche Doktrin des **fair use** bekannt);

  o Die **Persönlichkeitsrechte** des Urhebers;

  o Rechte anderer Personen, entweder am Lizenzgegenstand selber oder bezüglich seiner Verwendung, zum Beispiel für **Werbung** oder Privatsphärenschutz.

- **Hinweis —** Bei jeder Nutzung oder Verbreitung müssen Sie anderen alle Lizenzbedingungen mitteilen, die für diesen Inhalt gelten. Am einfachsten ist es, an entsprechender Stelle einen Link auf diese Seite einzubinden.

Genehmigt von der Philosophisch-Naturwissenschaftlichen
Fakultät auf Antrag von

Prof. Dr. Daniel Loss

Dr. P. Staňo

Basel, den 10. Dezember 2013   Prof. Dr. J. Schibler
                                                                          Dekan

Acknowledgments

It is a pleasure to express my gratitude for the support during the creation of this thesis.

First of all, I would like to thank Daniel Loss for giving me the unique opportunity to pursue my PhD as a member of his group. His experience and intuition, which enable him to ask the right questions and to propose intriguing ideas, both inspired me and provided excellent guidance. The cooperative environment as well as the enjoyable atmosphere within the condensed matter theory group are his achievements.

I am grateful to my collaborator, co-supervisor and mentor during my first project, Bernd Braunecker. Due to his vast knowledge he is able to loosen up lectures with fascinating anecdotes and motivate students to dive deeper into the field of condensed matter theory, including me. I would also like to thank my collaborator Franziska Maier for productive discussions, pleasant conversations as well as culinary exchange. I appreciate Peter Staňo for being co-referee.

The last four years were the most eventful and exciting years of my life. I am glad to have spent my time in such a friendly environment of group members, regular visitors and friends. I would like to thank Samuel Aldana, Daniel Becker, Dan Bohr, Christoph Bruder, Martin Brühlmann, Stefano Chesi, Charles Doiron, Mathias Duckheim, Carlos Egues, Gerson Ferreira, Jan Fischer, Suhas Gangadharaiah, Rahel Heule, Adrian Hutter, Daniel Klauser, Jelena Klinovaja, Christoph Klöffel, Franz Knuth, Viktoriia Kornich, Verena Körting, Jörg Lehmann, Dmitrii Maslov, Tobias Meng, Simon Nigg, Andreas Nunnenkamp, Christoph Orth, Fabio Pedrocchi, Diego Rainis, Hugo Ribeiro, Maximilian Rinck, Beat Röthlisberger, Arijit Saha, Manuel Schmidt, Thomas Schmidt, Constantin Schrade, Pascal Simon, Dimitrije Stepanenko, Vladimir M. Stojanovic, Grégory Strübi, Rakesh Tiwari, Björn Trauzettel, Mircea Trif, Luka Trifunovic, Filippo Troiani, Yaroslav Tserkovnyak, Oleksandr Tsyplyatyev, Andreas Wagner, Stefan Walter, Ying-Dan Wang, James Wootton, Robert Zak, and Alexander Zyuzin.

Summary

Current computer systems encode data in sequences of the binary unit, the bit. The quest of designing faster processors is one of the most important in modern society. However, reducing the size of transistors and thus CPUs is limited to the size of single atoms. Modern fabrication techniques employed in industry achieve structures at scales down to 22nm. Hence, new computation schemes are necessary to continue construction of better processors. Expanding the properties of the bit is a scheme widely spread in the condensed matter community. The most promising ansatz is to enable the bit to not only take states 0 and 1 but also any superposition of the two and thus providing a new set of operations. Essentially, this concept takes the bit into the world of quantum mechanics and marks the genesis of the qubit. Numerous proposal for the implementation of the qubit exist. However, an electron spin confined to a quantum dot (QD) turns out to be the most natural realization of the qubit. Hence, knowledge of QD properties is essential to the fabrication of an efficient and powerful quantum computer.

In the first part of this thesis we study a QD tunnel coupled to one dimensional conductors (1D), in particular edge states of fractional quantum Hall (FQH) samples. Our proposed setup combines two regimes that individually attract tremendous scientific effort. The QD is in the Coulomb blockade regime. Hence sequential tunneling processes from edge state via the QD to the other edge state are suppressed. Thus, we focus on cotunneling, i.e. second order processes transferring a particle directly from one edge to the other. 1D conductors are strongly correlated systems that reveal interesting elementary excitations. Especially FQH edge states at filling factor 5/2 have been identified to exhibit excitations obeying non-Abelian statistics. Renormalization group calculations show that the relevant excitations are quasiparticles of both quarter and half of the elementary charge. We determine the cotunneling conductance via the QD for different kinds of charge carriers, in particular electrons and quasiparticles of fractional charge $e/2$ and $e/4$. On the one

hand, we find that the electron cotunneling conductance is strongly suppressed while on the other hand both e/2 and e/4 quasiparticles exhibit distinctive signatures in the cotunneling lineshapes. Our findings provide a test of the Moore-Read wavefunction based on a simple transport measurement.

The second part is devoted to the response of a qubit to external fields. In particular, we study the electron spins confined to self-assembled InAs QDs of pyramidal shape. We present a trial wavefunction obeying hard-wall boundary conditions for a pyramidal geometry. Starting from the band structure of the bulk material we model the QD by adding strain and hard-wall confinement potential according to the considered geometry. Furthermore, we account for external electric and magnetic fields. We decouple the conduction band from the valence band and find the spectrum of the bound electron states in the QD. Finally, we extract the g factor and analyze the dependence on the direction of the external fields. Depending on the respective electronic states, we find a variety of g factor anisotropies suitable for determination by a simple transport measurement. We find both qualitatively good agreement with recent measurements and shapes not yet observed in experiments. At last, we conclude that our findings can be employed to control the splitting of qubit states and therefore should prove useful for qubit manipulation.

Contents

Appendix

Introduction

In this chapter we briefly set the foundation for the thesis. We elaborate on the evolution of atom models and show basic properties of electrons orbiting nuclei in Sec. 1.1. We then present the discovery of quantum dots in condensed matter physics and discuss similarities to atoms, see Sec. 1.2. In Sec. 1.3, we outline how the spectrum of a quantum dot is obtained from the bulk band structure. We further elaborate on the importance of quantum dot research and give a brief introduction to edge states of the quantum Hall effect in Secs. 1.4 and 1.5, respectively. Finally, we give the outline of this thesis, see Sec. 1.6.

1.1 Atom models

The curiosity of mankind has always been fueled by the quest for the unknown and especially the smallest constituents of matter. As an example for the drive to discover smaller and smaller particles, we give the famous excerpt of Dr. Heinrich Faust's monologue in Johann Wolfgang von Goethe's tragic play [Goe05]:

> That I may detect the inmost force
> Which binds the world, and guides its course.

Faust is pushed towards the verge of insanity by his insatiable curiosity. Although we refrain from taking as extreme measures, we still continue

to maximize our understanding of nature in all its greatness. For the
purpose of the thesis at hand the above statement shall be limited to the
concept that atoms consist of nuclei and electrons. Further subdivison
of the nuclei goes beyond the scope of this work, even beyond of this
field. To avoid a head start, we give a brief overview on atom models
ranging from the first concept of indivisible particles in ancient Greece to
implementation of quantum mechanics in the 20th century.

The Greek philosopher Democritus lived around 400 BC and was an
important character in the history of atomic models [D13]. Democritus
and his teacher Leucippus were probably the first to postulate that all
matter consists of small particles called atoms. In addition they stated
that these atoms are not divisible any further, i.e. smaller constituents or
subatomic particles are non-existent. From this ground breaking concept
we take a rather large leap in time which brings us to the 20th century
[TN01]. The British Physicist Sir Joseph John Thomson discovered that
cathode rays consist of negatively charged particles which lead him to
the idea that there is more to atoms than known so far. In 1903 Thom-
son postulated an atom model with two kinds of constituents. Electrons
of negative charge are distributed in a positively charged, uniform sea
that fills the entire volume of the atom with diameter 1Å. For the dis-
tribution of the electrons he used the pictures "raisins in a muffin" or
"plums in a pudding" which suggest a static understanding of the atom.
However, the electrons are not localized as in the pictorial descriptions
but move freely within the atom. We note that the atom in the so-called
Thomson model contains no nucleus but a homogenic background. Only
ten years later, in 1913, Ernest Rutherford pointed a beam of alpha par-
ticles, i.e. helium nuclei, at a thin gold foil and observed a wide range
of deflection angles, in particular up to π. In the Thomson model the
alpha particles pass the gold foil built from a uniform sea of positive
charge with electrons embedded within accompanied by minor deflec-
tions. However, the experiment exhibits strong deflection not plausible
within the Thomson model. These findings suggested a model in which
the positive charge of the atom is confined to a small nucleus at the center
of the atom and in which electrons are orbiting the nucleus. The space
in between neighboring nuclei is empty such that an alpha particle is
able to pass the foil without interacting with the nuclei. However, when
an alpha particle approaches a nucleus, it can be deflected in any direc-
tion depending on the exact trajectory. In this new picture the electrons
are bound to the nuclei by the Coulomb interaction and orbit in vacuum
around the nuclei. A problem arose in this picture. An electron on a cir-
cular trajectory emits radiation, thus looses energy and hence collapses

into the nucleus. In 1913 Niels Bohr postulated that radii of electrons orbiting a nucleus take discrete rather than arbitrary values such that the properties of the discrete radii supersede classical mechanics. Thus, the electron states in an atom are energetically quantized and the quantization is given by the angular momentum L which is an integer multiple of a fixed unit, $\hbar$. Bohr laid the foundation for an atom model that changed our understanding of nature. In 1924 Louis de Broglie postulated that all particles have wave character with the wavelength given by their respective momenta. The wavelength assigned to a macroscopic particle is short compared to its size such that a double slit interference experiments prove to be impossible due to the small separation of the two slits. Electrons, however, are subject to the laws of quantum mechanics and exhibit wave character. Thus, electrons moving on a closed orbit require periodic boundary conditions according to the concept of standing probability waves. De Broglie found that the radii of the electron orbits in the Bohr model agree with the concept of standing probability waves with periodic boundary conditions. In 1926 Erwin Schrödinger postulated the famous relation between the energy and the wavefunction of a particle or state

$$H \left| \psi \right\rangle = E \left| \psi \right\rangle, \tag{1.1}$$

with energy operator H and eigenenergy E of state $\left| \psi \right\rangle$. In fact H is a differential operator and the Schrödinger equation is a partial differential equation whose solutions, wavefunctions $\left| \psi \right\rangle$, describe the properties of the particle or state. The solutions to the Schrödinger equation of the hydrogen atom yield the electron density distributions, the so-called orbitals. The energy of electrons confined in these orbitals increases for decreasing extents of the wavefunction which is equivalent to increasing the attractive potential. This is easily understood when regarding Werner Heisenberg's uncertainty principle of 1927

$$\Delta x \, \Delta p \geq \frac{\hbar}{2}, \tag{1.2}$$

where Δx and Δp are inverse proportional to each other and with the spatial extent of the wavefunction Δx and the extent in momentum space Δp which is closely related to the kinetic energy. Further effects such as the exact size, structure and charge distribution of the nucleus and interaction among electrons affect the orbitals of the electrons as well. However, the description of atoms explained so far is sufficient for the purpose of this thesis.

In summary, electrons orbiting around a positive core are spatially confined due to the Coulomb potential generated by the nucleus. The

following section gives a brief overview on artificially constructed condensed matter systems that exhibit energetically quantized electron states in analogy to atoms according to the discussion above.

1.2   Artificial atom-like structures - QDs

Point-like, i.e. zero dimensional (0D), objects in condensed matter physics where single elementary charges can be trapped are called quantum dots (QDs). In this section, we present the discovery of QDs as well as the analogy between atoms and quantum dots, also referred to as artificial atoms.

In 1987 T.A. Fulton and G.J. Dolan [FD87] performed simple conductance measurements that brought a whole new research field to existence. A thin electrode, of size 50×800 nm^2 was tunnel coupled to three leads and capacitatively coupled to a backgate controlling the chemical potential of the central electrode. Two leads acted as source and drain of electrons, while the third one was used to determine the capacitance of the electrode during the transport measurement. From the measured capacitance they deduced the electron number on the electrode. The measurements were performed on different samples with varying size of the electrode. For smaller electrodes the *I-V* curve exhibited oscillations that were absent for larger electrodes. The oscillation appeared for varying backgate voltages when the charging energy, E_C, overweighed the bias voltage applied to source and drain, V. The charging energy is a kind of energy penalty or entry fee an electron has to pay in order to tunnel onto the electrode, i.e. the QD [Ihn10]. Furthermore, the charging energy, $E_C = e^2/C$, is characterized by the capacitance of the island, C, which is directly correlated to the size of the electrode, and with elementary charge e. Hence, the spectrum of the electrode is given by equidistant levels with splitting E_C. Depending on the size of the island the QD spectrum is dominated by different energy scales. In large structure the charging energy is the dominant energy scale compared to quantum mechanical confinement effects and the level distance is equidistant. For decreasing QD sizes the confinement increases until it ultimately dominates the energy spectrum of the QD. In few electron QDs quantum effects dominate. Clearing the QD from all electrons, i.e. depletion, as well as adding of single electrons is easily achievable by tuning the backgate voltage accordingly. We note that the number of electrons on a QD is well-defined. When investigating the energy required to add another electron to the QD, an atomic, orbital-like structure is revealed, see Fig.

18.19 in [KAT01]. The detailed spectrum can be probed by a simple transport measurement. Transport through the QD is enabled when one or more energy levels of the QD spectrum lie within the bias window given by source and drain, in particular the bias voltage is larger than the level splitting at the Fermi surface of the leads. Every QD level in the bias window yields a channel for electron transport through the QD. When no QD level lies within the bias window such that the level splitting at the Fermi surface of the leads is larger than the bias voltage, sequential tunneling processes are suppressed and the QD is in Coulomb blockade.

Tremendous scientific effort has been spent on a rich variety of QD topics in condensed matter research such as decoherence, long-distance spin-spin coupling, spin-orbit coupling, spin-dependent tunneling, spin relaxation, spin dephasing, hyperfine interaction, as well as lateral gate defined, self-assembled, vertical and nanowire QDs. For reviews see Refs. [KL13, HKP$^+$07, FMAE$^+$07].

In the most basic sense both QDs and atoms are objects that confine electrons spatially to a point-like volume, i.e. 0D, exhibiting quantum effects in the spectra and electron probability densities. However, a major difference is the symmetry of the confining potential. While atoms exhibit a highly symmetric potential, the potential of QDs strongly depends on type and shape of the QDs. This is both advantage and challenge. On one hand the QDs can be designed to match the required properties of a device. On the other hand fabrication of a QD with perfect size and symmetry is a great challenge, since the positioning of electrodes, edging of semiconductor heterostructure, etc. on the nm scale is subject to mesoscopic effects, here mesoscopic side effects.

1.3   From bulk semiconductors to QDs

QDs are built from semiconductor heterostructures and some bulk properties that affect the QDs such as g factor, effective mass, coupling to low-lying hole bands, spin-orbit coupling, and the band gaps strongly depend on the specific semiconductor materials. Knowledge of the bulk band structure is therefore essential for detailed investigation of QD properties. The most prominent semiconductor materials in condensed matter research are III-V semiconductor compounds such as gallium arsenide (GaAs) and indium arsenide (InAs).

Theoretical description of electrons in bulk semiconductors is achieved through $\boldsymbol{k} \cdot \boldsymbol{p}$ theory which is based on the Schrödinger equation, see Eq. (1.1), for a periodic lattice and the associated Bloch functions

[Win03]. $\boldsymbol{k} \cdot \boldsymbol{p}$ theory delivers powerful tools for the analysis of semiconductor band structures. The most important feature is that the discussion can be limited to a specific band or set of bands. An established approach is to focus on the bands close to the gap between conduction band (CB) and valence band (VB), i.e. the lowest conduction band, heavy- and light-hole bands, and the split-off band. Depending on the respective band gaps, high-lying conduction bands and low-lying valence bands are not taken explicitly into account. However, effects of these distant bands enter through modified band structure parameters. A QD is modeled by accounting for a strong confinement potential in the bulk Hamiltonian. The confinement induces a splitting of the bands into subbands according to the spectrum of the QD as discussed in Sec. 1.2. Furthermore, influences from external fields, magnetic, paramagnetic, and strain-induced interactions can be included into $\boldsymbol{k} \cdot \boldsymbol{p}$ theory by adding the corresponding terms to the Hamiltonian. At the interfaces of different semiconductor materials, e.g. at the boundary of an InAs QD embedded in a GaAs matrix, the lattice is highly strained due to mismatch of the respective lattice constants. The modified lattice constants relax to their bulk values for increasing distances from the interface. However, a QD is surrounded by such interfaces, thus depending on the QD size the lattice within the QD may not relax. Strain which is strongly shape dependent causes a displacement of the charge density that in turn reduces the symmetry of the QD and affects anisotropic quantities such as the g factor. Finally, we outline a proper approach to obtain the electronic spectrum of a QD from the band structure of the bulk. The bulk Hamiltonian is expressed in an expanded basis due to the subband splitting. The CB is decoupled from the VB by means of a Schrieffer-Wolff transformation such that a projection on the CB yields an effective CB Hamiltonian. Diagonalization of the effective CB Hamiltonian reveals the eigenenergies of the CB levels in the QD and hence the spectrum of the electronic states in the QD.

1.4   Importance of QD research

One of the most ambitioned goals of the condensed matter research field is the creation of a quantum computer, i.e. a computer exploiting quantum effects such as superposition in calculation and data storage to speed up the computation process [KL13]. In classical computers data is stored encoded in the basic computational unit bit. Since the bit is a binary quantity, it can be mapped onto a two level system such as a spin in a magnetic field [LD98]. The two eigenstates of S_z up and down, $|\uparrow\rangle$ and

$|\downarrow\rangle$, are assigned to 0 and 1, respectively. However, a spin is not limited to the two eigenstates but can assume any superposition, i.e. any point on the Bloch sphere is possible. This quantum mechanical effect can be exploited when manipulating the state of the spin such that some operations or algorithms speed up exponentially. Thus a bit formed by a quantum mechanic two level system is called a qubit. Spatial localization of individual spins is favorable due to a simplified selection of the processed spin. Since design and construction of QDs are mature technologies, localization of spins can be readily achieved in QDs, double QDs, and arrays of QDs. Circuits integrating quantum processors operating on qubits can be realized. However, the response of spins to perturbations such as external fields is under ongoing investigation, see Ch. 3. QDs are very versatile objects whose properties such as spectrum, g factor, spin relaxation and decoherence times depend on material, shape, coupling to leads or gates, interaction, external fields both strength and direction, and so forth. Some effects differ from one state to the next excited state. Providing the opportunity of controlling single particle tunneling as well as tuning the QD levels enables exploitation of spin blockade, i.e. inhibition of transport of one spin direction. Thus, QDs can be employed as spin filters generating a spin polarized current [RSL00].

Semiconductor devices provide favorable realizations of quantum processors due to scalability of the heterostructures and maturity of the research field. Furthermore, QDs reveal natural implementations of qubits as well as a variety of phenomena exploitable for qubit operations.

1.5 Electrons in two dimensions

In general individual electrons subject to magnetic fields exhibit various effects such as cyclotron movement, spin precession, Zeeman splitting defining the g factor, and so forth. The list grows as one adds two dimensional (2D) confinement, a strong out of plane magnetic field and low temperatures to the list of ingredients.

Electrons moving in a magnetic field are subject to the Lorentz force deflecting the electrons perpendicular to both momentum and magnetic field [Jai07]. The circular trajectory is characterized by the cyclotron radius $r = p_\perp/eB$ with momentum $p_\perp$ perpendicular to the magnetic field, positive elementary charge e, and magnetic field B. A two dimensional conducting sample reveals a voltage perpendicular to the direction of the current when exposed to an out of plane magnetic field. The so called Hall voltage stems from the deflection of the electrons by the Lorentz

force. For increasing magnetic fields the radii describing the motion decrease until at low temperatures and high magnetic fields the radii eventually reach values much smaller than the extents of the sample. A phase transition from classical to quantum mechanics occurs such that the circular motion is subject to periodic boundary conditions. The constraints cause quantization of the electron energy as well as formation of Landau levels. The quantization emerges in analogy to the Bohr atom model, see Sec. 1.1. In finite samples the circular movement of electrons close to the edge, i.e. closer than the cyclotron radius, is interrupted. These edge electrons start moving along the edge of the sample such that chiral edge channels emerge. The movement of an electron in a one dimensional (1D) channel is restricted by its neighboring electrons such that motion is only possible in a collective manner since evasion is impossible. In the resulting collective state electrons are not well-defined. However, the problem of interacting fermions can be mapped onto non-interacting bosons such that the fermion field operator is described by an exponential of the boson field operator. Furthermore, the resulting Hamiltonian is quadratic in the bosonic fields independent of the interaction. Hence, the technique to describe 1D conductors in Luttinger liquid theory is called bosonization [Gia04, Jai07]. The Hall conductivity through the 1D edge channels of a quantum Hall sample is given by

$$\sigma_H = \nu \, \frac{e^2}{h},\tag{1.3}$$

with elementary charge e, and Planck constant h. The filling factor ν takes integer or fractional values characterizing the integer (IQHE) and fractional quantum hall effect (FQHE), respectively. We note that the Hall conductivity and resistivity reveal plateaus at integer and fractional filling factors when tuning the magnetic field. The FQHE is observed at certain strong magnetic fields that induce interactions between the electrons in addition to 2D confinement and low temperatures. The electrons then condense into the lowest Landau levels and enter a collective state. Hence, the elementary excitations of the system are of collective nature and considered quasiparticles of fractional charge which is correlated to the filling factor ν. These quasiparticles consist of magnetic flux quanta attached to a charge, hence called composite fermions. The FQHE can be understood as an IQHE of composite fermions. Such quasiparticles usually obey neither bosonic nor fermionic exchange statistics. On the exchange of two quasiparticles with Abelian statistics a phase is acquired. Furthermore, quasiparticles exist that obey non-Abelian statistics that cannot be described by a simple phase. Non-Abelian particles

exhibit potential to prove useful for applications in topological quantum computations.

1.6 Outline

The thesis at hand is structured as follows. In the first part we combine two very different phenomena of low dimensional structures in condensed matter physics in a simple transport measurement. A QD in the Coulomb blockade regime is tunnel coupled to 1D edge states of FQH samples. We investigate signatures of the Moore-Read state in quasiparticle transport in the $\nu = 5/2$ FQH regime where we focus on cotunneling processes. The discovered lineshapes of the cotunneling conductance can be easily verified by a simple transport measurement. Furthermore, our findings are also applicable to Laughlin edge states.

In the second part we investigate g factor anisotropy in self-assembled InAs QDs. Furthermore, we propose a trial wavefunction for a pyramidal QD with hard-wall confinement. We model an InAs self-assembled QD using 8-band $\boldsymbol{k} \cdot \boldsymbol{p}$ theory. We start from the bulk band structure and account for strain and confinement according to the pyramidal geometry. We find the spectrum of the CB states in the QD in dependence of the applied magnetic field. Finally, we extract the g factors of the lowest CB levels and find anisotropies with respect to the magnetic field direction. Our findings support the idea of qubit manipulation by means of g tensor modulation.

Part I

Quasiparticle transport

Quasiparticle cotunneling

We show that cotunneling in the 5/2 fractional quantum Hall regime allows us to test the Moore-Read wave function, proposed for this regime, and to probe the nature of the fractional charge carriers. We calculate the cotunneling current for electrons that tunnel between two quantum Hall edge states via a quantum dot and for quasiparticles with fractional charges $e/4$ and $e/2$ that tunnel via an antidot. While electron cotunneling is strongly suppressed, the quasiparticle tunneling shows signatures characteristic of the Moore-Read state. For comparison, we also consider cotunneling between Laughlin states, and find that electron transport between Moore-Read states and between Laughlin states at filling factor 1/3 have identical voltage dependences.

2.1   Introduction

Fractional quantum Hall (FQH) states are intriguing states of matter because elementary collective excitations behave as quasiparticles with fractional charge and statistics. The FQH state at filling factor 5/2 (5/2-FQHS) has become of special interest because it has been identified in several proposals as a state in which the elementary excitations obey

non-Abelian fractional statistics [MR91, FNTW98, RR99, RG00, LRNF07, LHR07, NSS$^+$08]. Numerical simulations testing these proposals have remained inconclusive [Mor98, RH00, FRNDS08, FRY$^+$09, MS08, ZHR09], mainly due to finite size limitations. A proof of the nature of the 5/2-FQHS should therefore come from experiments [RMM$^+$08]. As a first indicator, evidence for a chiral Luttinger liquid at the edges of the FQH sample was obtained in Ref. [MRZ$^+$07], demonstrating the fractional nature of the quantum state, yet not its Abelian/non-Abelian statistics. It has also been shown that quantum point contacts and interferometers can be constructed in the samples [JCS$^+$03, SBS$^+$99], allowing for the implementation of the interferometer-based tests proposed in Refs. [LFG06, FK06, FGK$^+$07, WF10]. A thermoelectric probing of different FQH states on quantum dots has been proposed in Ref. [VDGS12]. Yet further proposals for tests are desirable to obtain conclusive evidence. Theoretical FQH studies have shown that quantum dot (QD) and quantum antidot (AD) structures with corresponding excitations, electrons, and quasiparticles (QPs), exhibit similar physics [dCCFK$^+$97, GL97]. In the cotunneling regime the number of particles on the dot is conserved and second order tunneling processes dominate transport [AN92, GL04]. Elastic (inelastic) processes conserve (change) the state of the dot. The inelastic process leads to an excitation of the dot for bias voltages larger than the level spacing on the dot. Since the implementation of dot structures has become a mature experimental technique, we propose in the present paper a QD based setup for an alternative test of the nature of the 5/2-FQHS. In particular, we show that the cotunneling current strongly depends on the nature of the elementary QP excitations that can contribute to the current that is allowed to tunnel through the dots.

Possible charge carriers are electrons and fractionally charged QPs with non-Abelian statistics. The most prominent candidate QPs are excitations of charge $e/4$ and $e/2$ with e being the electron charge [FFN07, BN08, DHU$^+$08, VYPW11, CFB$^+$11, CFB$^+$12]. We investigate the existence of signatures of the 5/2-FQHS according to the theoretical description proposed by Moore and Read (MR) [MR91] in simple transport measurements, e.g., conductance through a QD.

Figure 1 shows the two situations of interest: (a) two different FQH samples at filling factor $\nu = 5/2$ which are weakly tunnel coupled to a QD, and (b) one single FQH sample whose edge states are weakly tunnel coupled to an AD in the bulk. The tunneling particles in the latter are non-Abelian QPs instead of electrons. The edge states are modeled by a chiral Luttinger liquid theory [Wen90, Wen92, Wen95, Gia04, GNT04] corresponding to the MR state whose eigenmodes are fractional excita-
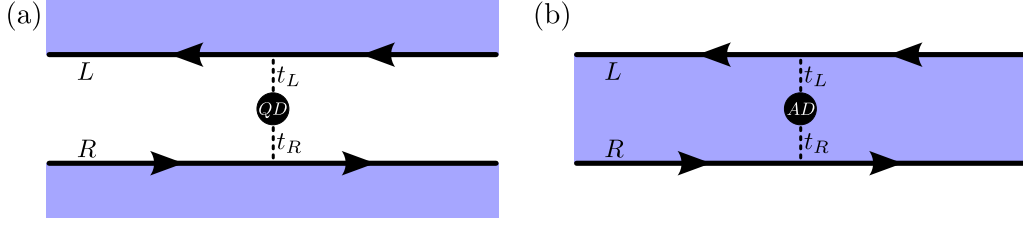
Figure 2.1: Sketch of the two setups considered in this work: Moore-Read edge states L and R, at chemical potentials $\mu_{L,R}$, tunnel coupled to (a) a quantum dot (QD) and (b) a quantum antidot (AD). The shaded (blue) region represents the bulk of the FQH samples. In setup (a) tunneling is limited to electrons, while in (b) the quasiparticles (QP) that can tunnel are determined by the filling factor of the AD, and, for the MR state both, charge-$e/2$ and -$e/4$, QPs are possible.

tions. In this work we focus on cotunneling in the Coulomb blockade regime close above a sequential tunneling peak such that it is energetically favorable to first remove a particle from the dot rather than first adding another particle. An interesting outcome of our calculation is that electron cotunneling via a QD between both Laughlin edge states at filling factor $\nu = 1/3$ and MR edge states shows the same bias voltage dependence.

2.2 Result

The cotunneling current from lead l to lead l' in lowest order in the bias V is given by $I = I_{el} + I_{inel}$, with I_{el} being the elastic cotunneling current given by

$$I_{el} = \frac{2\pi}{\hbar} \frac{\left(\frac{V}{\Lambda}\right)^{2\kappa-2}}{\Gamma(2\kappa)} \frac{\gamma_l \gamma_{l'} V}{(\mu_l - \varepsilon_{nq})^2} \, \theta(V), \tag{2.1}$$

and I_{inel} the inelastic cotunneling current given by

$$I_{inel} = \frac{2\pi}{\hbar} \frac{\left(\frac{V-\Delta}{\Lambda}\right)^{2\kappa-2}}{\Gamma(2\kappa)} \frac{\gamma_l \gamma_{l'} (V - \Delta)}{(\mu_l - \varepsilon_{nq})^2} (1 + \rho^*) \, \theta(V - \Delta), \tag{2.2}$$

with bias $V = \mu_l - \mu_{l'}$, chemical potential μ_l of edge state l, single-particle level spacing on the dot $\Delta = \varepsilon_{n'q} - \varepsilon_{nq}$, dot level ε_{nq}, effective bandwidth of the leads $\Lambda = \hbar u/\alpha$ (bounded by the gap of the 5/2-FQHS) defining the length α, velocity of the bosonic (fermionic) edge excitations u (v_n), Heaviside step function θ, and tunneling rate $\gamma_l = |A_{ln'n}|^2/(2\pi v_n \hbar)$ with

$A_{ln'n} = \sum_p t_{lp} \langle n' | d_{pq} | n \rangle$ (see below). The renormalized dot occupation $\rho^* \propto (V + \Delta)^{2\kappa-1} - (V - \Delta)^{2\kappa-1}$ accounts for the overshooting of the conductance close to the transition from the elastic to the inelastic regime and will be given in detail below. The parameter κ is determined by the type of tunneling particles (see below). For cotunneling of $e/2$ and $e/4$ QPs in setup (b), we replace the step function θ by the Fermi function $f(V) = \left(1 + e^{V/k_B T}\right)^{-1}$ (for a temperature $T < \Delta/k_B$ and the Boltzmann constant k_B) which smooths out the discontinuities at $V = 0, \Delta$ for $T = 0$, and we use the $V \to \sqrt{V^2 + (k_B T)^2}$ regularization for cotunneling of $e/4$ QPs.

2.3   Model

The system is modeled by the Hamiltonian $H = H_0 + H_T$, where $H_0 = H_L + H_R + H_D$ describes the uncoupled FQH edges and the dot, and H_T the tunneling between them. In the considered systems the leads are fractional quantum Hall edge states modeled according to the MR state and described by the Hamiltonian for lead l at chemical potential μ_l [MR91, FFN07]

$$H_l = \frac{u\hbar}{2\pi} \int dx \left(\partial_x \phi_l(x)\right)^2 - iv_n\hbar \int dx \, \eta_l(x)\partial_x \eta_l(x), \qquad (2.3)$$

where ϕ_l is a chiral boson field, the Majorana field η_l is the zero mode, and $u \, (v_n)$ is the velocity of the bosonic (neutral fermionic) excitations. For the MR state the lower filled Landau level acts as a background potential and causes a shift of the energy levels which is not important in our discussion. The fermion operator in lead l is given by [FFN07, Wen95]

$$\psi_{le}(x,t) = \frac{e^{-ik_1 x}}{\sqrt{2\pi\alpha}} \, \eta_l(x,t) \, e^{i\phi_l(x,t)\sqrt{2}}, \qquad (2.4)$$

with k_1 proportional to the particle density in the leads. Analogously the $e/2$ and $e/4$ QP operators are [FFN07, Wen95, FFN06]

$$\psi_{l\frac{e}{2}}(x,t) = \frac{e^{-ik_1 x}}{\sqrt{2\pi\alpha}} \, e^{i\phi_l(x,t)/\sqrt{2}}, \qquad (2.5)$$

$$\psi_{l\frac{e}{4}}(x,t) = \frac{e^{-ik_1 x}}{\sqrt{2\pi\alpha}} \, \sigma_l(x,t) \, e^{i\phi_l(x,t)/2\sqrt{2}}, \qquad (2.6)$$

where σ_l is a chiral Ising spin field.   The dot is modeled by $H_D = \sum_n \varepsilon_{nq} d_{nq}^\dagger d_{nq}$, where d_{nq} is the electron or QP operator for the discrete particle level n on the dot similar to Eqs. (2.4), (2.5), and (2.6) with

particle charge $q = e$ for electrons on the QD and $q = e/2, e/4$ for QPs on the AD. The Coulomb repulsion of the particles lifts a possible degeneracy of the energy levels including both charging and interaction energies. Tunneling between the leads and the dot is described by the perturbation $H_T = \int dx \sum_{l,n} t_{ln} \psi_{lq}^\dagger(x) d_{nq} + h.c.$, where $\psi_{lq}(x)$ and d_{nq} annihilate particles of charge q in lead l at x and in the dot level n, respectively, and with tunneling amplitude t_{ln}. From Ref. [FFN07] we know that QP tunneling processes are dominant in the MR state.

In setup (a) (Fig. 2.1) the leads are independent as they belong to different FQH systems. Independence between the edges is also assumed in setup (b), which requires that the length of the edges be larger than the coherence length of the excitations, estimated as $2.3l_0$ with $l_0 \sim 4\mu m$ being the magnetic length [BZBS09, WHRY08]. Tunneling in the leads is assumed to be limited to the positions closest to the dot, denoted by $x = 0$ with width $\Delta x \ll k_1^{-1}$, because t_{ln} depends exponentially on the tunneling distance [RL02] and consequently no special effects arise from the difference in velocities between bosons and Majorana states as opposed to Mach-Zehnder interferometers [LFG06, FK06, FGK$^+$07, WF10]. We focus on the Coulomb blockade regime, where the particle number on the dot is fixed, $N_q = \sum_n d_{nq}^\dagger d_{nq}$. The charging energy of the dot is much larger than the single-particle level spacing Δ and particularly larger than $\mu_l - \varepsilon_{nq}$. Tunneling processes through energetically distant dot levels are suppressed. The dot forms an effective two-level system that contains one particle. The persistence of the ground state in the elastic regime is ensured by charge conserving cotunneling processes which relax the state of the dot. The charge of the tunneling QPs is set by the filling factor of the AD such that there is no mixing of $e/4$ and $e/2$ QPs. We consider a regime in which the applied bias and the level spacing on the dot are larger than the temperature, allowing us to essentially neglect temperature effects. Since the MR state is spin-polarized, spin is neglected in the model [Mor98, RH00, FRY$^+$09, CL08, TGKM12, SPV$^+$12] and the fermion operator ψ_{le} is identified with the spin-polarized electron.

2.4 Transition rates

The transition rate $W_{l'l}(n', n)$ of transferring a particle from lead l to lead l' and shifting the particle on the dot from level n to level n' is determined

by the golden rule

$$W_{l'l}(n', n) = \frac{2\pi}{\hbar} \sum_{|F\rangle \neq |I\rangle} \left| \langle F|\hat{T}|I\rangle \right|^2 \delta(E_I - E_F), \qquad (2.7)$$

with the T matrix $\hat{T} = H_T(E_I - H_0 + i0^+)^{-1}\hat{T}$, final, $|F\rangle$, and initial, $|I\rangle$, states for the two leads and the dot, and energies E_F, E_I respectively. Level broadening in the leads (reservoirs) is neglected in state $|F\rangle$. We focus on the second order in the tunneling Hamiltonian H_T and the cotunneling regime. The linear order of H_T in the T matrix leading to sequential tunneling is suppressed in the Coulomb blockade regime [AN92] such that only the next order, cotunneling, matters. The final and initial states are given by $|F\rangle = |F_l\rangle \otimes |F_{l'}\rangle \otimes |F_D\rangle$ and $|I\rangle = |I_l\rangle \otimes |I_{l'}\rangle \otimes |I_D\rangle$, with $|F_l\rangle = \psi_{lq} |I_l\rangle$, $|F_{l'}\rangle = \psi_{l'q}^\dagger |I_{l'}\rangle$, $|F_D\rangle = d_{n'q}^\dagger d_{nq}|I_D\rangle$, and initial lead l and dot states $|I_l\rangle$ and $|I_D\rangle$, respectively.

From Eqs. (2.4), (2.5), and (2.6) we obtain the correlation functions for electrons, $q = e/2$, and $q = e/4$ QPs, respectively, [Wen95]

$$\langle \psi_{le}^\dagger(t)\psi_{le}(0) \rangle = \frac{\langle \eta_l(t)\eta_l(0) \rangle}{2\pi\alpha} \, e^{2J(t)} \propto t^{-(\kappa=3)}, \qquad (2.8)$$

$$\langle \psi_{l\frac{e}{2}}^\dagger(t)\psi_{l\frac{e}{2}}(0) \rangle = \frac{1}{2\pi\alpha} \, e^{J(t)/2} \propto t^{-(\kappa=1/2)}, \qquad (2.9)$$

$$\langle \psi_{l\frac{e}{4}}^\dagger(t)\psi_{l\frac{e}{4}}(0) \rangle = \frac{\langle \sigma_l(t)\sigma_l(0) \rangle}{2\pi\alpha} \, e^{J(t)/8} \propto t^{-(\kappa=1/4)}, \qquad (2.10)$$

with $J(t) = -\ln\big((-ut + i\alpha)/i\alpha\big)$. The indicated power laws define the coefficient κ. The noninteracting case, $\kappa = 1$, corresponds to the Fermi liquid (FL) limit. We note that, since $x = 0$, the Majorana fermion field η_l (Ising spin field σ_l) results in a simple correlator, increasing the lead correlation exponent κ by 1 (1/8) such that $\kappa = 3, 1/2, 1/4$ for $q = e, e/2, e/4$, which is in contrast to the Mach-Zehnder interference proposals [LFG06, FK06, FGK+07, WF10] and leads to simpler propagators.

In the inelastic cotunneling regime, $V > \Delta$, processes exist which excite the dot and change the occupation probabilities of the dot levels. The steady state occupation probabilities are then determined by the master equation $W^\uparrow \rho(1) - W^\downarrow \rho(2) = 0$, with $W^\uparrow = \sum_{l,l'} W_{l'l}(2,1)$, $W^\downarrow = \sum_{l,l'} W_{l'l}(1,2)$, and $\rho(n)$ the occupation probability of level $n = 1, 2$. The cotunneling current from lead l to lead l' is then given by

$$I_{l'l} = \sum_{n,n'} W_{l'l}(n', n)\rho(n). \qquad (2.11)$$

The renormalized dot occupation in Eq. (2.2) reads $\rho^* = (W_{l'l}(1,2) - W_{l'l}(2,1))/(W^{\uparrow}+W^{\downarrow})$. We evaluate Eq. (2.7) by means of Fourier integration over time to reexpress the T matrix in terms of the correlators given in Eqs. (2.8)-(2.10). We then find for the cotunneling rates for charge transfer between FQH edge states and a dot

$$W_{l'l}(n',n) = \frac{2\pi}{\hbar}\,\Gamma_{l'ln'n}^{\kappa}\,\frac{\gamma_l\gamma_{l'}(V-\Delta)}{(\mu_l-\varepsilon_{nq})^2}\,\theta(V-\Delta), \qquad (2.12)$$

with the real coefficients

$$\Gamma_{l'ln'n}^{\kappa} = \left.\frac{\left(\frac{V-\Delta}{\Lambda}\right)^{2\kappa-2}}{\Gamma(2\kappa)}\right|_{l\neq l'} + \delta_{l',l}\,\Xi_{ln'n}^{\kappa}, \qquad (2.13)$$

where Γ is the Gamma function and $\Xi_{ln'n}^{\kappa}$ results from energy renormalization in the leads. In the limit of noninteracting leads, $\Gamma_{l'ln'n}^{1} = 1$ and hence $\Xi_{ln'n}^{1} = 1$, the FL result of Ref. [RSL00] close to a sequential tunneling resonance is recovered. For charge conserving processes of $e/2$ ($e/4$) QPs, $\Xi_{ln'n}^{1/2}$ ($\Xi_{ln'n}^{1/4}$) can be approximated by their most singular
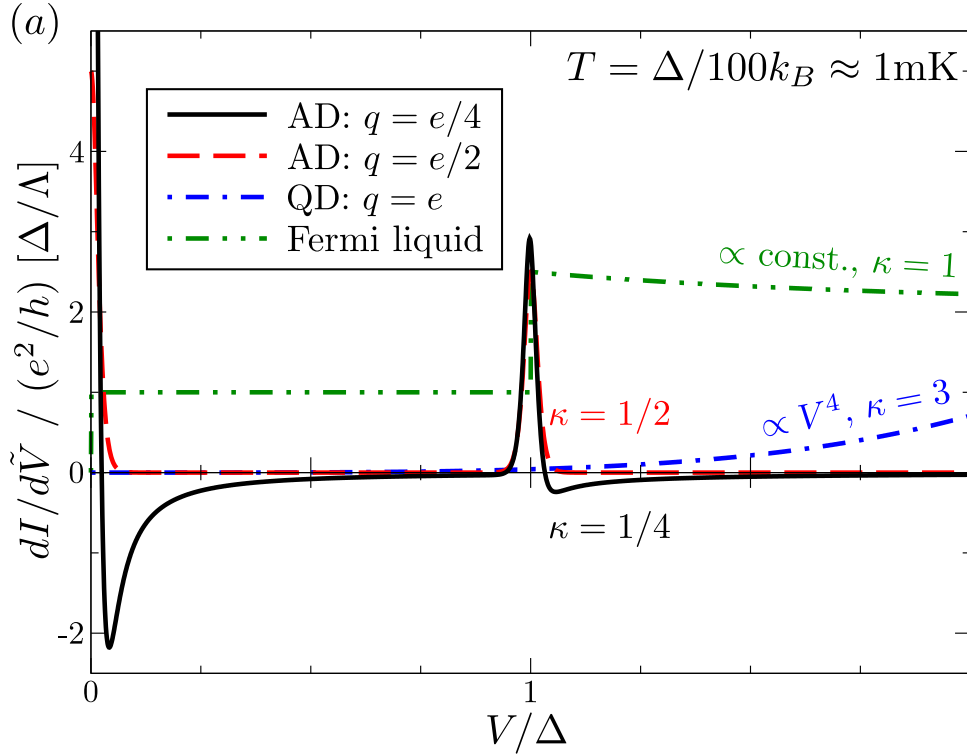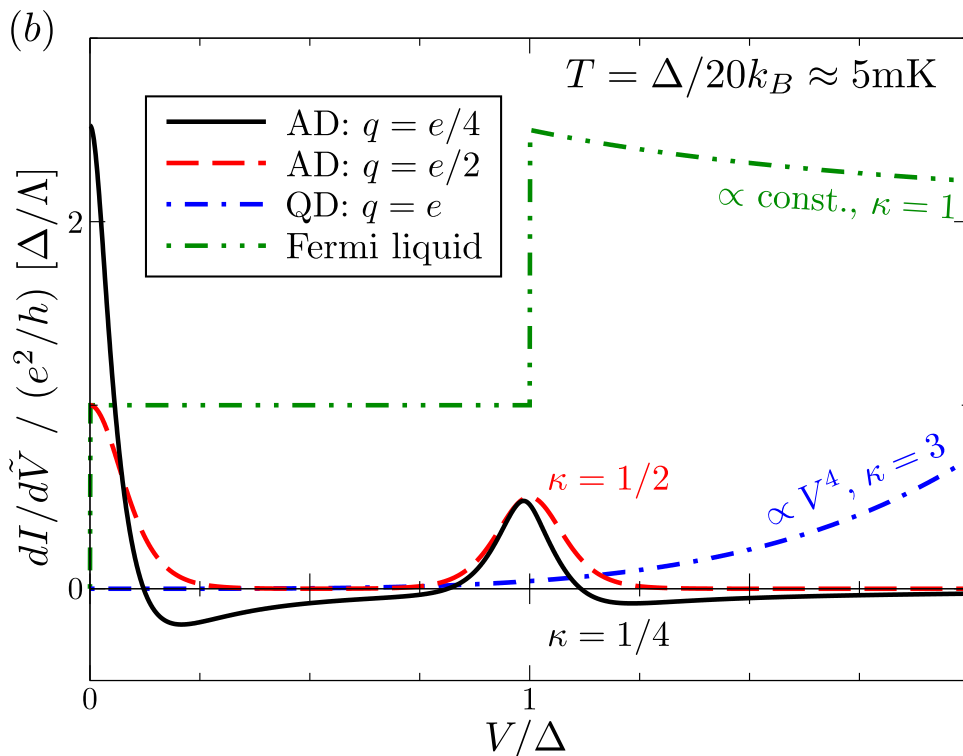
Figure 2.1: Cotunneling conductance $dI/d\tilde{V}$ with $\tilde{V} = V/e$, and $I = I_{el} + I_{inel}$ given by Eqs. (2.1) and (2.2) for $e/4$ and $e/2$ QP transport between MR edge states of the same FQH sample through an AD, electron transport between MR edge states of separate FQH samples through a QD, and electron transport between FL leads through a QD. The $e/2$ and $e/4$ QP conductance is shown for the temperatures (a) $T = \Delta/100k_B \approx 1$mK and (b) $T = \Delta/20k_B \approx 5$mK, respectively.

contributions, the branch points (branch cuts), such that $\Xi_{ln'n}^{1/2} = -\Lambda/\Delta$ ($\Xi_{ln'n}^{1/4} = |\Lambda/\Delta|^{3/2}/\sqrt{\pi}$), whereas for electron cotunneling processes $\Xi_{ln'n}^{3}$ results in a lengthy expression with, however, negligible effect. From Eqs. (2.11)-(2.13) we obtain the results of Eq. (2.1) (for $\Delta = 0$) and Eq. (2.2).

2.5   Discussion

We have calculated the cotunneling current of the MR state in both se-tups of electron and quasiparticle tunneling via a dot. The resulting line
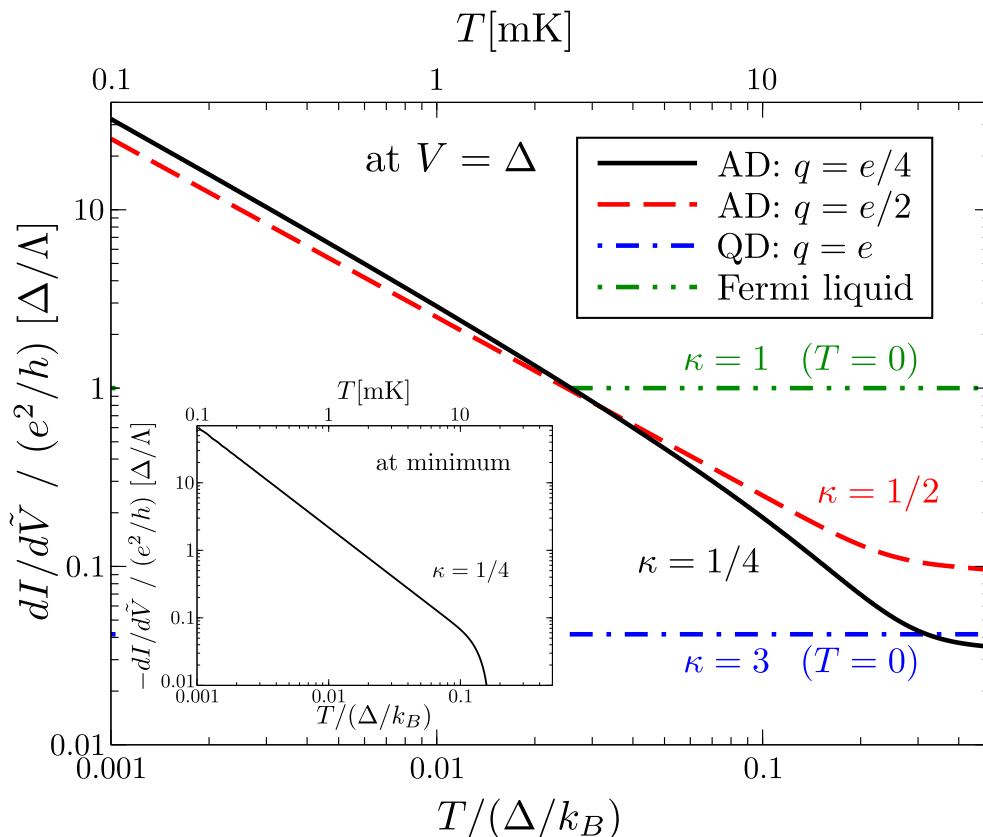
Figure 2.2: Temperature dependence of the $e/4$ and $e/2$ QP cotunneling conductance $dI/d\tilde{V}$ with $I = I_{el} + I_{inel}$ given by Eqs. (2.1) and (2.2) and $\tilde{V} = V/e$ fixed at the transition from the elastic to the inelastic regime, $V = \Delta$. Values for electron transport between MR edge states of separate FQH samples through a QD and electron transport between FL leads through a QD are shown for zero temperature. On the upper scales T is given in mK for $\Delta/k_B = 100$mK. The inset shows the conductance dip depth, $-dI/d\tilde{V}$, for $e/4$ QP tunneling at the minimum in the nonfixed bias V.

shapes differ significantly, especially from the line shape of the FL regime [GL04]. The cotunneling current for electrons shows a power law dependence on both the bias applied to the edge states and the effective bandwith of the leads, $V^{2\kappa-1}$ and $\Lambda^{2-2\kappa}$. The effective bandwidth Λ is on the order of the effective Landau level gap size in the 5/2-FQHS, $\sim$ 100-500 mK. We note that $\bar{\gamma}_l = \gamma_l \Lambda^{1-\kappa}$ can be considered an effective co-tunneling amplitude from which it is obvious that electron cotunneling

between MR edge states via a QD is highly suppressed by the fourth inverse power of the effective bandwidth, $\bar{\gamma}_L\bar{\gamma}_R = \gamma_L\gamma_R \, \Lambda^{-4}$, due to the fact that four $e/4$ QPs are forced to tunnel simultaneously, in agreement with earlier findings that electron tunneling is least relevant in the MR state [FFN07]. Figure 2.1 shows the differential conductance, dI/dV, in the cotunneling regime, for electron tunneling in the FL regime and in the MR state via a QD, and for $e/4$ and $e/2$ QP tunneling in the MR state via an AD at experimentally achievable temperatures, (a) $T = \Delta/100k_B \approx 1$ mK and (b) $T = \Delta/20k_B \approx 5$ mK, respectively. In the FL regime, which corresponds to noninteracting excitations of the FQH edge, previous results [RSL00, GL04] are recovered. Fig. 2.2 shows the temperature dependence of the $e/4$ and $e/2$ QP cotunneling conductance at the transition from the elastic to the inelastic regime, $V = \Delta$. The inset gives both the $e/4$ QP conductance dip depth, $-dI/d\tilde{V}$ at the minimum with respect to V, and the temperature range for which the negative differential conductance of $e/4$ QPs is observed. The MR state reveals its special signature in the line shape of the cotunneling conductance. For $e/4$ QP tunneling regions of negative differential conductance appear. On the other hand, both $e/2$ and $e/4$ QPs show pronounced conductance peaks at the opening of a new transport channel. These special peaks corroborate the findings of Ref. [FFN07] of $e/2$ and $e/4$ QP tunneling being relevant. In the cotunneling regime, however, the renormalization group flow is cut off by bias V and temperature T such that the perturbative result is accurate. Our calculations show that the different charge carriers can be clearly distinguished by standard transport measurements.

Our approach is also applicable to a setup of two separate FQH samples with common Laughlin FQH edge states at filling factor ν weakly coupled through a QD, similar to the setup in Fig. 2.1 (a). The cotunneling current is then given by Eqs. (2.1) and (2.2) with $\kappa = 1/\nu$ [Wen95]. In this scenario, $1/\nu$ QPs of fractional charge ν combine to a full electron charge when tunneling through the QD, such that not one particle has to tunnel but $\frac{1}{\nu} - 1$ additional particles. Due to the necessity of simultaneous tunneling the electron cotunneling current is suppressed by $\Lambda^{2-2/\nu}$. It is interesting to note that electron tunneling via a QD in both the MR state and the Laughlin state at filling factor $\nu = 1/3$ show the same voltage dependence. However, the two states differ in the velocities of the excitations due to the bosonic and fermionic nature of the lead eigenmodes.

In conclusion, we have shown that electron cotunneling via a quantum dot is strongly suppressed in the Moore-Read state compared to $e/4$ and $e/2$ quasiparticle cotunneling via an antidot. The line shape of the differential conductance reveals the special signature of the Moore-Read

state. Both the Moore-Read wave function can be verified and the charge carrying excitation can be determined by measuring the cotunneling current in the setups depicted in Fig. 2.1.

Part II

g factor anisotropy

CHAPTER 3

Pyramidal InAs quantum dots

We investigate the wave functions, spectrum, and g-factor anisotropy of low-energy electrons confined to self-assembled, pyramidal InAs quantum dots (QDs) subject to external magnetic and electric fields. We present the construction of trial wave functions for a pyramidal geometry with hard-wall confinement. We explicitly find the ground and first excited states and show the associated probability distributions and energies. Subsequently, we use these wave functions and 8-band $\boldsymbol{k} \cdot \boldsymbol{p}$ theory to derive a Hamiltonian describing the QD states close to the valence band edge. Using a perturbative approach, we find an effective conduction band Hamiltonian describing low-energy electronic states in the QD. From this, we further extract the magnetic field dependent eigenenergies and associated g factors. We examine the g factors regarding anisotropy and behavior under small electric fields. In particular, we find strong anisotropies, with the specific shape depending strongly on the considered QD level. Our results are in good agreement with recent measurements [Takahashi *et al.*, Phys. Rev. B **87**, 161302 (2013)] and support the possibility to control a spin qubit by means of g-tensor modulation.

3.1   Introduction

Electron spins confined to semiconductor quantum dots (QDs) are excellent candidates for the physical realization of qubits, the elementary units of quantum computation [LD98]. The qubit state can be initialized and manipulated by means of externally applied electric and magnetic fields. Thus knowledge about the qubit's response to these fields is crucial for the successful operation of qubits. This response depends strongly on the type of QD considered, e.g., lateral gate defined QDs, nanowire QDs, and self-assembled QDs [KL13, HKP+07]. The most prominent type of QDs for self-assembled QDs are InAs QDs grown on a GaAs surface or in a GaAs matrix. These QDs can be grown in various shapes such as pyramids [GSB95, GCL+95, RWS+95], truncated pyramids [LSG+96], and flat disks [BHH+01] and hence are highly strained due to the lattice constant mismatch of substrate and QD materials. In self-assembled InAs QDs, spin states have been prepared with more than 99% fidelity [ADB+06] and complete quantum control by optical means has been shown [PDGM+10, PLZY08]. However, full qubit control by means of external fields and small system sizes are the most important goals in solid state based quantum computation, allowing for the construction of integrated circuits [KL13, HKP+07]. Regarding these requirements, g-tensor modulation is a powerful mechanism that allows control of the qubit [PPF11, PPF08, BPC+13] but is sensitive to the shape of the QD hosting the qubit [HKP+07]. Hence the qubit behavior under the influence of geometry, external fields, etc., is still subject to ongoing scientific effort [TSL12, PMS+12, JMSS12]. A crucial ingredient for modeling the qubit behavior is the knowledge of the particle distribution within the QD, i.e., the envelope wave function which is mainly determined by the shape of the QD. For simple structures such as spheres, flat cylinders, and cubes, the wave functions in QDs can be described analytically, e.g., by employing hard-wall or harmonic confinement potentials [CTDL77]. For more complicated shapes usually numerical models are employed [GSB95, PPS97, Pry98, SGB99, DP07]. Recently, there have been efforts to find analytical wave functions for pyramids with different types of boundary conditions [HRV+12, VTH13]. However, the set of wave functions introduced so far has been observed to be incomplete, lacking for example the ground state wave function. Both analytical and numerical methods are employed to further explore QD characteristics such as strain [GSB95, ND10], spectra [GSB95], and g factors [PF06, PF07]. Explicit values depend on the material properties. Building QDs in materials with very large, isotropic bulk g factors, i.e., InAs ($g = -14.9$), is favorable due to an improved opportu-

nity of g-factor modification. Measurements emphasize the decrease of the g factor when considering electrons in InAs QDs. Numerical calculations [DP07, PF06, PF07] and measurements [BKF+99, MRPPM02] show that the g factor can go down to very small values and depends strongly on the dot size. Furthermore, recent measurements show a significant anisotropy [dFB+13, TDO+13] of the g factor which turned out to be tunable by electrical means [TDO+13, DKT+11]. This behavior of g can be attributed to material- and confinement-induced couplings between the conduction band (CB) and the valence band (VB) which result in totally mixed low-energy states.

The outline of this paper is as follows. In Sec. 3.2, we present an 8-band $\boldsymbol{k} \cdot \boldsymbol{p}$ Hamiltonian describing the low-energy QD states which accounts for strain and external electric and magnetic fields. Additionally, we introduce a set of trial wave functions satisfying the hard-wall boundary conditions of a pyramidal QD. Furthermore, we derive an effective Hamiltonian describing CB states in the QD. In Sec. 3.3, we present the results of our calculations, in particular the g-factor anisotropy of CB QD levels. These results are discussed and compared to recent measurements in Secs. 3.4 and 3.5, respectively. Finally, in Sec. 3.6, we conclude.
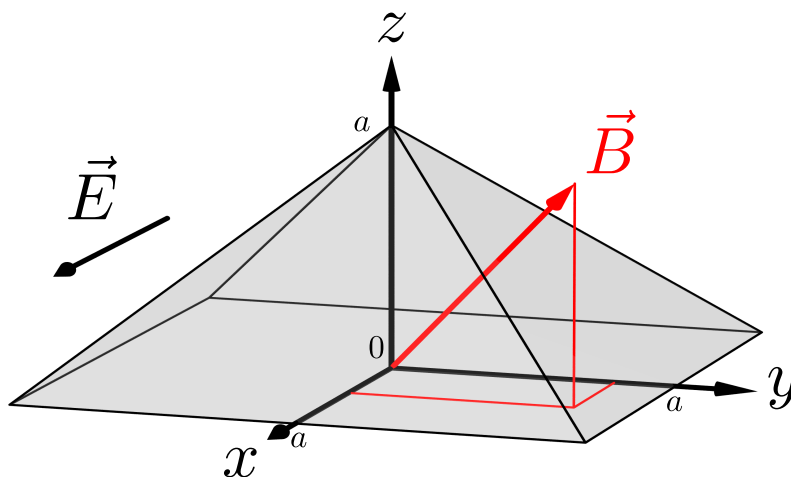

Figure 3.1: Sketch of the QD geometry and the coordinate system used in this work with x, y, and z axes pointing along the growth directions [100], [010], and [001], respectively. The externally applied fields under consideration are $\boldsymbol{B} = (B_x, B_y, B_z)$ and $\boldsymbol{E} = (E_x, 0, 0)$.

3.2   Model

In this section, we introduce the Hamiltonian and wave functions used in this work. Furthermore we outline the performed calculations and give the main results in a general manner.

3.2.1   Hamiltonian

Low-energy states in bulk III-V semiconductors are well described by an 8-band $\boldsymbol{k} \cdot \boldsymbol{p}$ model [Win03], which includes the CB and the VB consisting of heavy- (HH) and light-hole (LH) bands, and split-off (SO) bands. The associated Hamiltonian $H_{\boldsymbol{k} \cdot \boldsymbol{p}}$ is given in terms of two-fold degenerate basis states $|j, \pm\rangle$, $j = \mathrm{CB, HH, LH, SO}$, which are linear combinations of products of angular momentum eigenfunctions and real spin states [Win03]. We model a pyramidal QD by taking into account a three-dimensional hard-wall confinement potential V_c defining a square pyramid of height a and base length $2a$ as sketched in Fig. 3.1. We introduce strain by adding the strain Hamiltonian H_{strain} [Win03]. An analytical description of the strain distribution within an InAs pyramid enclosed in a GaAs matrix can be modeled by exploiting the analogy to electrostatic theory [ND10]. We include the effect of an externally applied magnetic field $\boldsymbol{B} = \boldsymbol{\nabla} \times \boldsymbol{A}$ defined by the vector potential $\boldsymbol{A}$ ($\boldsymbol{\nabla} \cdot \boldsymbol{A} = 0$) by adding two terms. The first term is the magnetic interaction term H_Z [Win03]. To derive the second term, H_B, we replace $\boldsymbol{k} \to \boldsymbol{k} + e\boldsymbol{A}/\hbar$ in $H_{\boldsymbol{k} \cdot \boldsymbol{p}}$ and H_{strain} in a semiclassical manner, where e is the positive elementary charge and $\hbar$ the Planck constant. We drop all contributions independent of $\boldsymbol{B}$ and obtain a Hamiltonian which accounts for orbital effects of $\boldsymbol{B}$. An external electric field $\boldsymbol{E}$ is included by adding the electric potential $H_E = e\, \boldsymbol{E} \cdot \boldsymbol{r}$, with $\boldsymbol{r} = (x, y, z)$. The full system is then described by the Hamiltonian

$$H = H_{\boldsymbol{k} \cdot \boldsymbol{p}} + H_{\mathrm{strain}} + H_Z + H_B + H_E + V_c. \tag{3.1}$$

Note that literature values for $\boldsymbol{k} \cdot \boldsymbol{p}$ parameters are usually given for 4-band models. In an 8-band model, the parameters have to be modified accordingly [Win03].

3.2.2   Hard-wall wave function

As a first step, we consider V_c of a pyramidal QD analytically and require a vanishing particle density at the boundaries. We construct a trial wave function satisfying these boundary conditions as follows.

The Schrödinger equation of a particle confined in a square with sides of length a with vanishing boundary conditions on the borders, has the well-known solution $\psi_{mn}^{\square}(x,y)$ with eigenenergies $E_{mn}^{\square}$. The wave function of a particle confined in an isosceles triangle obtained by cutting the square along the diagonal, $\psi^{\triangle}(x,y)$, is then constructed by linear combinations of degenerate solutions $\psi_{mn}^{\square}(x,y)$ while requiring a vanishing wave function at the diagonal of the square [Li84]. We span the full three-dimensional (3D) volume of the pyramid and the corresponding wave functions with the product of two such triangles and the associated $\psi^{\triangle}$. This consideration suggests then the following ansatz for the hard-wall wave functions inside the pyramidal geometry of the form

$$
\psi_{\boldsymbol{m}}(\boldsymbol{r}) = c \prod_{\xi=x,y} \Big[\sin\left(\alpha_\xi\, \xi^+\right) \sin\left(\alpha_z\, \xi^-\right)
$$
$$
\qquad - (-1)^{m_\xi+m_z} \sin\left(\alpha_z\, \xi^+\right) \sin\left(\alpha_\xi\, \xi^-\right) \Big],
$$
(3.2)

with $\boldsymbol{r} = (x,y,z)$, $c = \csc(\pi z)/N_{\boldsymbol{m}}$, $\alpha_i = m_i\pi/a$, $m_i = 1,2,3,\ldots$, $m_x \neq m_z$, $m_y \neq m_z$, $\boldsymbol{m} = (m_x, m_y, m_z)$, $\xi^\pm = \xi \pm (z-a)/2$, and $N_{\boldsymbol{m}}$ such that the integral over the pyramid volume $\int d^3r\, |\psi_{\boldsymbol{m}}(\boldsymbol{r})|^2 \equiv 1$. We define energies of $\psi_{\boldsymbol{m}}(\boldsymbol{r})$ by taking

$$
\frac{\hbar^2}{2m_0} \langle \psi_{\boldsymbol{m}}(\boldsymbol{r})| \, (-i\nabla)^2 \, |\psi_{\boldsymbol{m}}(\boldsymbol{r})\rangle = E_{\boldsymbol{m}},
$$
(3.3)

where m_0 denotes the bare electron mass. For notational simplicity we use $\psi_{\boldsymbol{m}} \equiv \psi_{m_x m_y m_z}$ and $E_{\boldsymbol{m}} \equiv E_{m_x m_y m_z}$. Exact analytical solutions of the Schrödinger equation have been derived using specular reflections of plain waves at the boundaries of the geometry [HRV+12]. However, the obtained set of solutions is incomplete, consisting solely of excited states and especially lacking the ground state. We stress that our ansatz $\psi_{\boldsymbol{m}}$ is not an eigenstate of the Schrödinger equation. However, the energies $E_{\boldsymbol{m}}$ we find are lower than the eigenenergies of the Schrödinger equation derived in Ref. [HRV+12]; see Secs. 3.3.1 and 3.4.1. In addition, the wave function for the lowest energy state, ψ_{221}, exhibits the expected nodeless shape for the ground state. A more detailed justification of $\psi_{\boldsymbol{m}}(\boldsymbol{r})$ is given in Appendix A. In the following calculations, we apply these trial envelope wave functions for both CB and VB states. In general, electron and hole envelope wave functions differ [GSB95, SGB99]; however, this choice is justified since we find that even this overly simplified picture yields already good results.

3.2.3 Zeeman splitting of the CB states in the QD

A strong confinement of the electron and hole wave functions to the QD, as assumed by taking V_c into account, corresponds to a splitting of the basis states into localized states which can be described as products of the former basis states and the confinement-induced envelope functions,

$$\Psi_{\boldsymbol{m}}^{j,\pm}(\boldsymbol{r}) = \psi_{\boldsymbol{m}}(\boldsymbol{r}) \left|j,\pm\right\rangle. \tag{3.4}$$

We note that a non-trivial set of basis states requires $\max\{m_j\} \geq 3$. We rewrite H in a basis formed by the $\Psi_{\boldsymbol{m}}^{j,\pm}$ by taking the according matrix elements and find a new Hamiltonian H_d describing the QD states. We split H_d into three parts,

$$H_d = H_d^{\mathrm{d}} + H_d^{\mathrm{bd}} + H_d^{\mathrm{bod}}, \tag{3.5}$$

where H_d^{d} denotes the diagonal elements of H_d, H_d^{bd} denotes the block-diagonal parts of H_d between the CB and VB, and H_d^{bod} the associated block-off-diagonal elements. The external electric and magnetic fields are treated as a perturbation to the system. Hence diagonal terms of H_d stemming from taking matrix elements of H_Z, H_B, and H_E are included in H_d^{bd}. Since we are interested in describing electrons confined to CB states of the QD, we decouple the CB states from the VB states by a unitary transformation, the Schrieffer-Wolff transformation (SWT) $\tilde{H}_d = e^{-S} H_d e^{S}$, where S is an anti-unitary operator ($S^\dagger = -S$) [Win03]. We approximate the SWT to third order in a small parameter λ determined by the ratio of the CB-VB coupling and the CB-VB energy gap. To this end, we express S as $S = S_1 + S_2 + S_3$, where $\mathcal{O}(S_i) = \lambda^i$. Here, the operators S_i are defined by $[H_d^{\mathrm{d}}, S_1] = -H_d^{\mathrm{bod}}$, $[H_d^{\mathrm{d}}, S_2] = -[H_d^{\mathrm{bd}}, S_1]$, $[H_d^{\mathrm{d}}, S_3] = -[H_d^{\mathrm{bd}}, S_2] - 1/3[[H_d^{\mathrm{bod}}, S_1], S_1]$ [Win03]. Since λ is small, we can expand e^S up to third order in λ using the decomposition of S. Assuming that $\mathcal{O}(H_d^{\mathrm{d}}) = \lambda^0$, $\mathcal{O}(H_d^{\mathrm{bd}}) = \mathcal{O}(H_d^{\mathrm{bod}}) = \lambda^1$, we perform the SWT where we keep terms up to third order in λ in the final Hamiltonian $\tilde{H}_d$. In a last step, we project $\tilde{H}_d$ on the CB and find an effective CB Hamiltonian, $\tilde{H}_d^{\mathrm{CB}}$. In $\tilde{H}_d^{\mathrm{CB}}$, the single QD levels are strongly coupled, and thus cannot be treated perturbatively anymore. Instead, we diagonalize $\tilde{H}_d^{\mathrm{CB}}$ exactly and evaluate the eigenenergies $E_n^{\pm}$, where the indices denote the nth QD level from the VB edge with effective spin $\pm$. We find the g factor of the nth spin-split QD level by taking
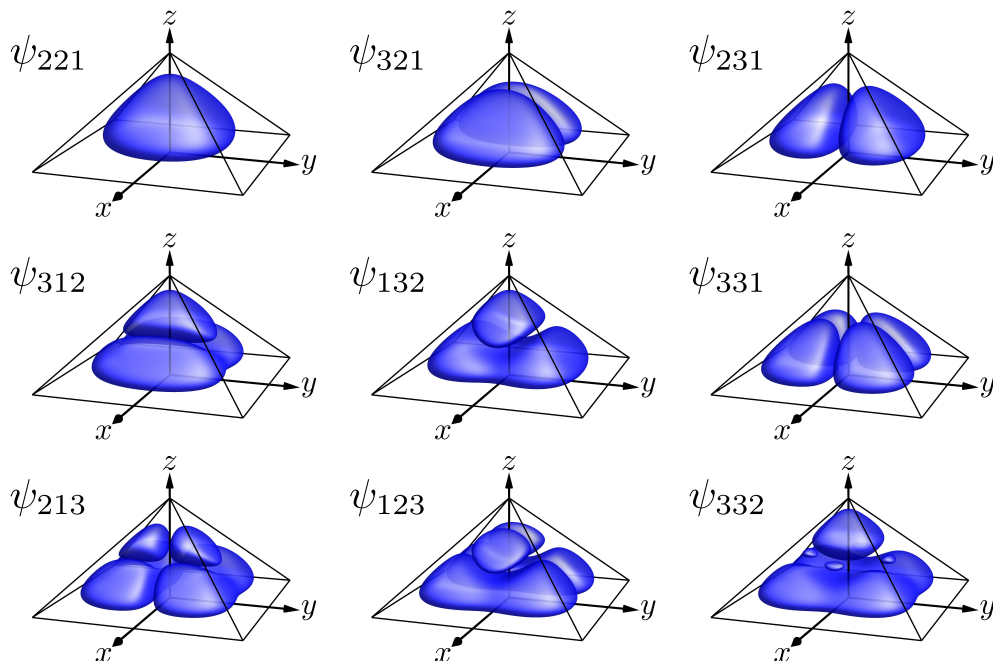
$$g_n = \frac{E_n^+ - E_n^-}{\mu_B |\boldsymbol{B}|}, \tag{3.6}$$

Figure 3.2: Probability distributions of the smallest nontrivial set of trial wave functions $\psi_{\boldsymbol{m}}(\boldsymbol{r})$, i.e., $\max(m_i) = 3$, satisfying the hard-wall boundary conditions for the geometry given in Fig. 3.1. We show contour plots of $|\psi_{\boldsymbol{m}}(\boldsymbol{r})|^2 = 0.1$ inside the pyramidal geometry assumed for the QD; see Fig. 3.1. Note the degenerate pairs: ψ_{321} and ψ_{231}, ψ_{312} and ψ_{132}, ψ_{213} and ψ_{123}.

with Bohr magneton μ_B. Since the exact values of the energies $E_n^{\pm}$ depend on the magnitude and direction of the external fields $\boldsymbol{E}$ and $\boldsymbol{B}$, $g_n = g_n(\boldsymbol{E}, \boldsymbol{B})$. $\tilde{H}_d^{\mathrm{CB}}$ contains higher order terms in $\boldsymbol{B}$; thus we find

$$g_n = g_{n,0} + g_{n,2}|\boldsymbol{B}|^2, \tag{3.7}$$

which is consistent with the general behavior expected of $\tilde{H}_d$ under time reversal. However, with $|g_{n,2}| \ll |g_{n,0}|$, the quadratic dependence of g_n on $|\boldsymbol{B}|$ is barely measurable in experiments.

3.3 Results

In this section, we present the results of the calculations outlined in Sec. 3.2. All calculations were performed for a pyramidal QD of height $a = 50$ nm. We consider basis states that fulfill $\max\{m_i\} \leq 3$, which re-

sults in a splitting of each band $|j, +\rangle$ ($|j, -\rangle$) into nine QD levels. The system parameters used for the Hamiltonians are listed in Table B.1 in Appendix B, where the notation directly corresponds to the notation used in Ref. [Win03].

3.3.1 Probability distribution of the wave function

We show contour plots of the probability distribution $|\psi_{\boldsymbol{m}}(\boldsymbol{r})|^2$ of the wave function found in Eq. (3.2), see Fig. 3.2. We present the lowest-energy states forming the smallest nontrivial set of wave functions. The ground state ψ_{221} with associated ground state energy $E_{221} = 0.53$ meV exhibits s-wave character; i.e., we find a single density cloud roughly fitting the pyramidal shape. For excited states, nodes appear in the center of the pyramid and along the axes of the coordinate system. We observe p-wave character for the states ψ_{321}, ψ_{231}, ψ_{312}, and ψ_{132}; see Fig. 3.2. The wave functions $\psi_{m_i m_j m_k}$ and $\psi_{m_j m_i m_k}$ with $m_i \neq m_j$ are degenerate and we find that the associated particle densities are of the same form, only with nodes oriented along different axes, i.e., x and y. Further restrictions arising from the pyramid geometry, such as correlations between the coordinates, result in symmetries regarding the quantum numbers, $\psi_{m_i m_i m_j} = \psi_{m_j m_j m_i}$.

3.3.2 Spectra of the CB states in the QD

In Fig. 3.3, we plot the energy spectrum of the low-energy CB states given by $\tilde{H}_d^{\text{CB}}$ and examine the behavior of the QD levels as functions of $\boldsymbol{B} = (0, 0, B_z)$. For $|\boldsymbol{B}| = 0$, we find six degenerate QD levels E_n which split into pairs while increasing $\boldsymbol{B}$ from 0 to 1 T, where we assume that $\boldsymbol{E} = 0$. Confinement and strain push the QD levels far apart from each other; hence the $\boldsymbol{B}$-induced spin splitting cannot be observed in the full plot, Fig. 3.3 on the left. To circumvent this, we produce magnified plots showing the $\boldsymbol{B}$ dependence of the single QD levels n, Fig. 3.3 on the right. We note that the splitting of the CB levels, $E_{n+1} - E_n$, is on the order of 100 meV which contrasts the Zeeman splitting, $E_n^+ - E_n^-$, which is on the order of 1 meV or below. For most QD levels $E_n^\pm$, we observe a clearly nonlinear dependence on $\boldsymbol{B}$, indicating a diamagnetic shift of the QD levels [vBSK$^+$12]. This dependence is not independent of the direction of $\boldsymbol{B}$, resulting in an anisotropy associated with the g factor; see Sec. 3.3.3.

3.3.3 g factor of the CB states in the QD

We discover strong anisotropies for the g factors of electrons confined to low-energy CB states of pyramidal shaped InAs QDs. The g factors of the first six QD levels from the VB edge, g_n with $n = 1, \dots, 6$, are shown as 3D plots and cuts along specific planes in Figs. 3.4 to 3.8 in ascending order. We calculate the g_n for magnetic fields of strength $|\boldsymbol{B}| = 1$ T. We further apply electric fields of strengths $|\boldsymbol{E}| = 0$ V/m and $|\boldsymbol{E}| = 10^6$ V/m along the x axis. In response to an electric field along the x axis the anisotropy axis slightly tilts away from the z axis. To reduce calculation effort, we interpolate between data points, however, we have checked consistency in several cases with non-interpolated plots.

We find anisotropies of various shapes and directions depending on the QD level under consideration. We observe the emerging of three main axes of anisotropy, $x + y$, $x - y$, and z, pointing along crystallographic directions $[110]$, $[1\bar{1}0]$, and $[001]$, respectively. QD levels $n = 1, 4, 6$ ($n = 2, 3$) reveal g-factor maxima along the $x+y$ (z) axes, whereas small g-factor values tend to appear along(in) the $x - y$ axis (xy plane). Along the $x - y$ axis we observe that a special situation arises for $n = 1$; here g approaches a very small value close to but still larger than zero. However, this drop depends strongly on the dot size; see Sec. 3.4.3. Interestingly, g_5 barely exhibits any anisotropy with maximum values at the $x + y$ axis and minimum values at the $x - y$ axis; see Fig. 3.7. This is in contrast to g_6, where we note a considerable increase of the g-factor values and again a significant anisotropy. Note the change of the color scale in Fig. 3.8. In general, we observe a dependence of the absolute values of the g_n on the QD size; see Sec. 3.4.3.

3.4 Discussion

In this section, we comment on the probability distributions of pyramidal QDs calculated in Sec. 3.3.1. Furthermore, we discuss the $\boldsymbol{B}$ dependence of both spectrum and g factor of the CB states in the QD presented in Secs. 3.3.2 and 3.3.3, respectively.

3.4.1 Probability distribution of the wave function

The wave functions of the lowest states exhibit the structure of cuboidal wave functions adapted to the pyramidal shape of the enclosing QD. We definitely observe the ground state as well as excited states. This is consistent with the method used for the construction of the wave functions.

Note that the wave functions $\psi_m(\boldsymbol{r})$ are not exact eigenfunctions of the Schrödinger equation. However, the boundary conditions are satisfied and the corresponding energies, see Eq. (3.3), are smaller than the energies of known analytical solutions of the Schrödinger equation provided that the correct boundary conditions are taken into account [HRV$^+$12]. Due to the method of construction, we find that the wave functions do not vanish at the diagonal planes $(x+y)z$ and $(x-y)z$, respectively, as was observed in Ref. [HRV$^+$12]. Furthermore, the authors of the work presented in Ref. [HRV$^+$12] explicitly state that the obtained set of wave functions is incomplete; solutions with a finite density at the center of the pyramid are not contained. In particular, a distinct ground state is missing. From this we conclude that our set of wave functions is more suitable to describe low-energy states in pyramidal QDs. Numerical calculations of QD wave functions usually include piezoelectric potentials and specific material properties directly from the beginning, which complicates a direct comparison [GSB95, SGB99]. However, compared to numerical calculations without strain as performed in Ref. [GSB95], where the wave functions extend into a wetting layer, and Ref. [SGB99], where no intermixing with a wetting layer is observed, we report similar shapes of the probability distributions with our analytical ansatz. Even though we apply this simplistic model, we recover the effects recently observed in experiments to a very good degree [TDO$^+$13]; see Sec. 3.4.3.

3.4.2   Spectra of the CB states in the QD

After diagonalizing $\tilde{H}_d^{\mathrm{CB}}$, we find states in the CB of the QD which are degenerate for $|\boldsymbol{B}| = 0$ and split into pairs by an increasing magnetic field. These energy levels exhibit a quadratic dependence on $\boldsymbol{B}$. We note that the direction of the magnetic field is important to the exact behavior of the splitting of the QD levels. Due to the highly admixed nature of the final eigenstates of $\tilde{H}_d^{\mathrm{CB}}$, which consist of CB and VB states of the basis introduced for H_d in Eq. (3.5), we find ourselves unable to comment on the exact shape of the nth eigenfunction. For illustrative plots of the electron wave function in considerably (one order of magnitude) smaller QDs from numerical and experimental studies, we refer the interested reader to Refs. [SGB99] and [VLP$^+$00].

3.4.3 g factor of the CB states in the QD

The reported anisotropy in our system stems from several effects. The first effect is the mixing of CB and VB states caused by the confinement

potential and intrinsic material parameters of the QD. This mixing is further influenced by the second effect, a change of gaps between the bands $|j, \pm\rangle$ due to strain. The intrinsic strain fields in the QD impose additional constraints on the system yielding a reduction of the symmetry of the level splitting with respect to the direction of $\boldsymbol{B}$. Furthermore, the strain fields reduce the symmetry class of the pyramid along the z axis from C_4 to C_2 [GSB95]. This reduction of the symmetry class agrees well with the observed anisotropy of the g_n in our work. Additionally, effects due to the orbital coupling of $\boldsymbol{B}$ may have an effect on g. For $|\boldsymbol{B}| = 1\,\mathrm{T}$, we find that the magnetic length $l_B = \sqrt{\hbar/e|\boldsymbol{B}|} \sim 25\,\mathrm{nm}$ is much smaller than the dot size characterized by $a = 50\,\mathrm{nm}$; hence Landau levels form. However, we took this into account by including H_B into our Hamiltonian; see Eq. (3.1). Compared to experimental results [TDO$^+$13], we observe very small g factors, mainly $g_n < 2$. However, small g factor values, in particular a zero crossing of g due to the transition from the bulk value $g_{\mathrm{bulk}} \approx -14.9$ to the free electron value $g_{\mathrm{free}} = +2$, have also been reported for circular and elliptical InAs QDs [PF06, PF07]. This transition is characterized as a function of the band gap between the CB and VB in the QD. In fact, we find a comparable magnitude of the g-factor values considering the band gap present in our system. In general, decreasing the QD size leads to a decrease of the CB-VB admixture and the g-factor values ultimately yield the free electron value, $g_{\mathrm{free}} = +2$. On the other hand, when increasing the QD size the g-factor values will finally approach the bulk value, $g_{\mathrm{bulk}} \approx -14.9$. Considering these two limits and assuming that the g factor is a continuous quantity, zero values of g will be observed eventually [PF06, PF07].

3.5 Comparison to experiment

In this section, we compare our results to recent experimental observations of the three-dimensional g-factor anisotropy in self-assembled InAs QDs by Takahashi *et al.*; see Ref. [TDO$^+$13]. The anisotropy of the QD g factor is usually extracted by transport measurements for different magnetic field directions [TDO$^+$13, dFB$^+$13]. The basic setup of these experiments consists of a QD which is tunnel coupled to two leads. An additional back-gate creates an electric field parallel to the growth direction. The back-gate voltage is used to select the QD level participating in the transport by changing the chemical potential of the QD. Furthermore, the tunneling rates depend on the different g factors of QD and

leads [SJ10]. We first point out that the QD considered in Ref. [TDO+13] is rather a half pyramid due to the applied gates. Thus, deviations of the absolute value of g compared to our findings are not unexpected. Such deviations increase even further due to different dot sizes. However, we find good qualitative agreement when accounting for the different confinement geometries in the following way. One can perform a coordinate transformation in order to align the axes of the upright pyramid considered above and the half-pyramid of Ref. [TDO+13]. Indeed, a rotation of $135°$ around the y axis aligns the symmetry axes of both systems in first approximation. We observe now that the g-factor anisotropies of the QD levels $n = 2, 3$ (Fig. 3.5) agree well with regions I and II of the charge stability diagram reported by Takahashi *et al.* in Ref. [TDO+13]. In region III they also find a state with a spherical distribution of the g factor similar to our calculation for QD level $n = 5$. Furthermore, they report measurements of a symmetrically covered upright pyramid as well. In this case the axes and shapes of the anisotropy are directly comparable to our results. The associated g-factor anisotropy agrees well with our findings for QD levels $n = 2, 3$. In general, due to confinement and strain, the QD size and shape have a strong influence on characteristic quantities such as spectrum and g factor, both absolute value and anisotropy. However, we find good qualitative agreement between our model calculation and the measurements. This is not surprising since both consider square-based pyramids which conserve the main anisotropy axes independent of the QD size. Finally, we point out that our model further predicts different shapes of the g-factor anisotropy depending on the QD levels – in particular, shapes not yet observed in experiments, such as the ones described for the QD levels $n = 1, 4, 6$.

3.6   Conclusion

In conclusion, we have found trial wave functions satisfying hard-wall boundary conditions for a pyramidal QD geometry. We calculated the associated particle density distributions of the low-energy states and found a ground-state-like, s symmetric state of lowest energy, as well as excited states with nodes along the coordinate axes of the system and at the center of the QD. We argued that these wave functions provide a good basis for analytical calculations of QD states. Furthermore, we have presented 8-band calculations to derive the spectrum of low-energy CB states in the QD. The magnetic field induced splitting of the QD levels shows a non-linear dependence on the magnetic field and strong anisotropies depend-

ing on the direction of the field. Starting from this, we have calculated the g factor of low-energy electrons in self-assembled InAs QDs subject to externally applied electric and magnetic fields. We calculated the g factor for all possible spatial orientations of the magnetic field and found distinct anisotropies. In particular, we showed that the anisotropies include configurations where the g factor drops down to values close to zero. Furthermore, we observed that the shape of the anisotropies depends on the QD level n and that the maximal values of g_n increase with n. Finally, we showed that our results are in good qualitative agreement with recent measurements. From these findings we conclude that the direction of magnetic fields applied to QDs can be used to control the splitting of qubit states efficiently and hence should prove useful for the manipulation of qubits in such QDs.
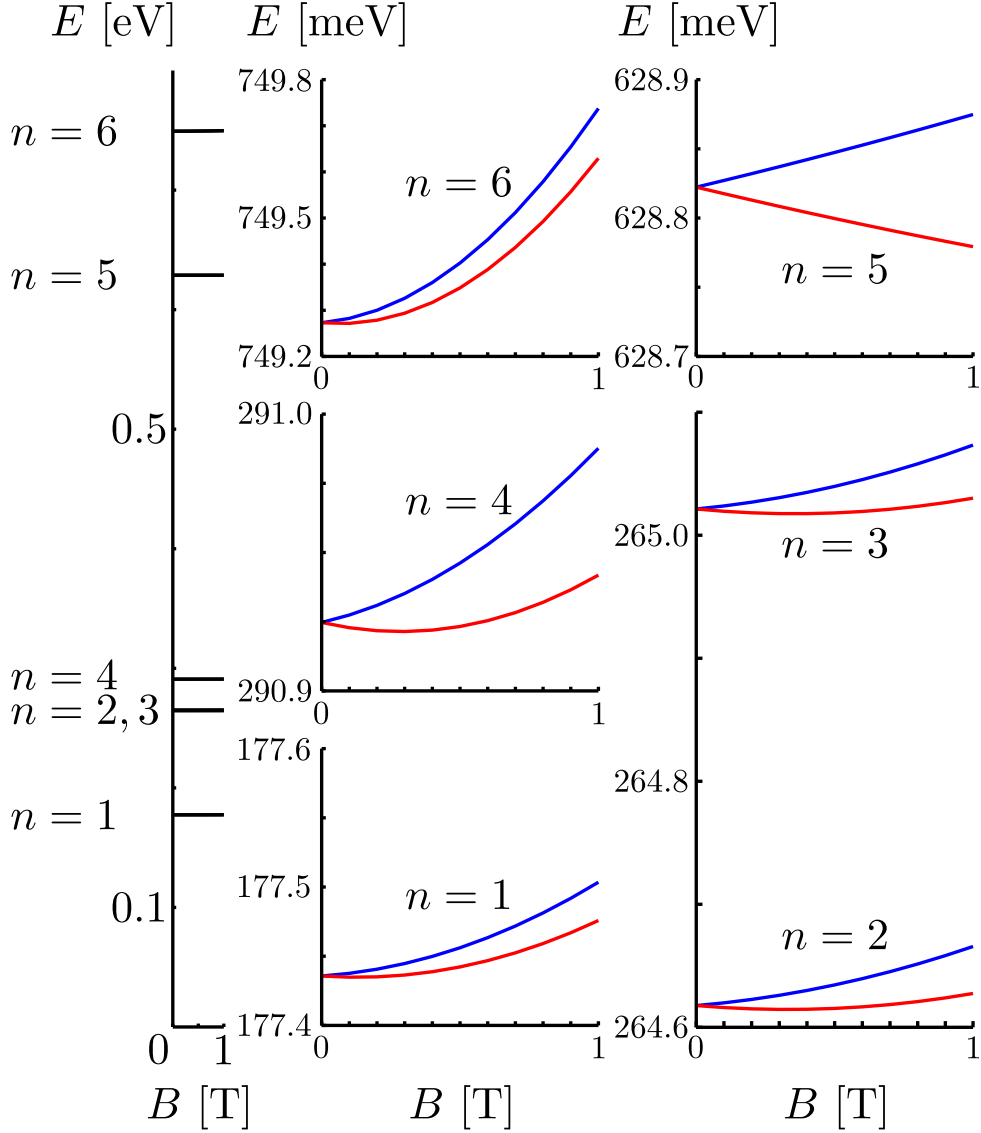
Figure 3.3: Left: Spectrum of the lowest six QD levels E_n of $\tilde{H}_d^{\mathrm{CB}}$ as a function of the magnetic field $\boldsymbol{B} = (0, 0, B_z)$, where we increase $|\boldsymbol{B}| = 0$ T to 1 T. We assume $\boldsymbol{E} = 0$. Right: Enlarged plots of the $\boldsymbol{B}$-dependent splitting of the single QD levels. For most QD levels, except for $n = 5$, we observe a nonlinear dependence of $E_n^{\pm}$ on $\boldsymbol{B}$.
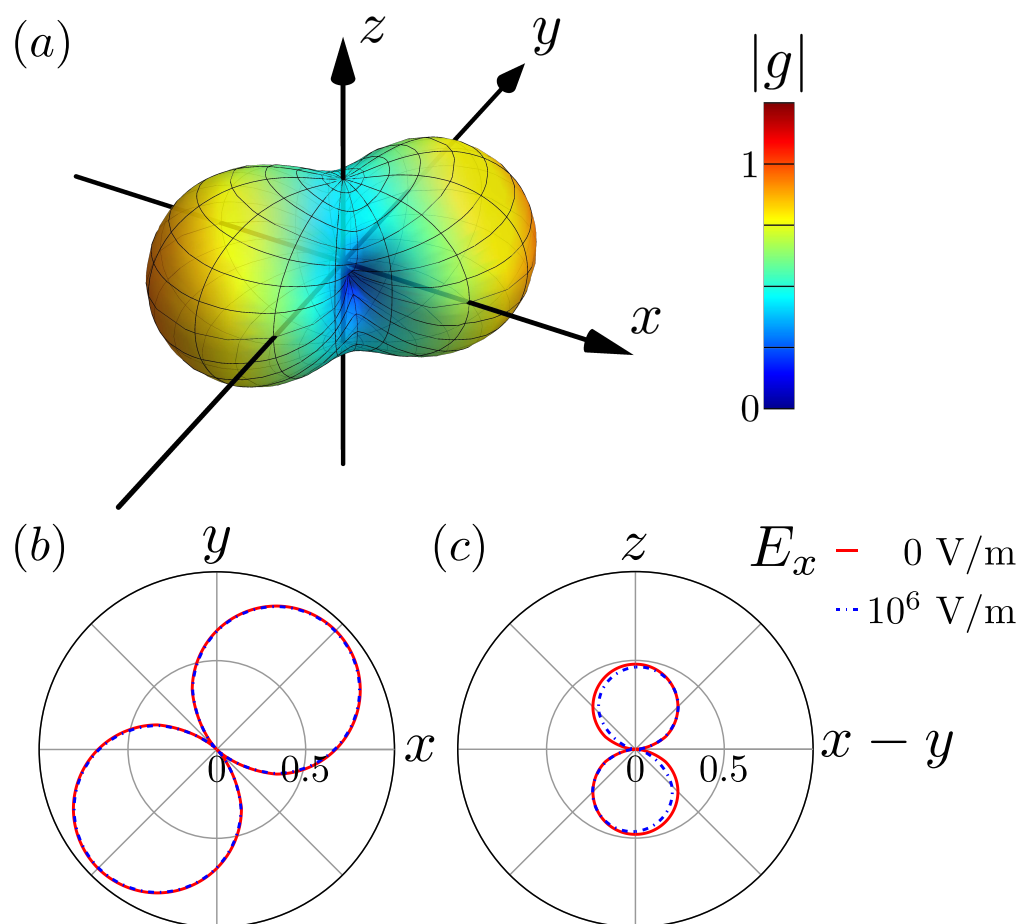
Figure 3.4: Ground state g factor $|g_1|$ as a function of the magnetic field direction for $|\boldsymbol{B}| = 1\,\mathrm{T}$ shown in (a) 3D plot, and cuts along the planes (b) xy, and (c) $(x-y)z$ with electric field $\boldsymbol{E} = (E_x, 0, 0)$.
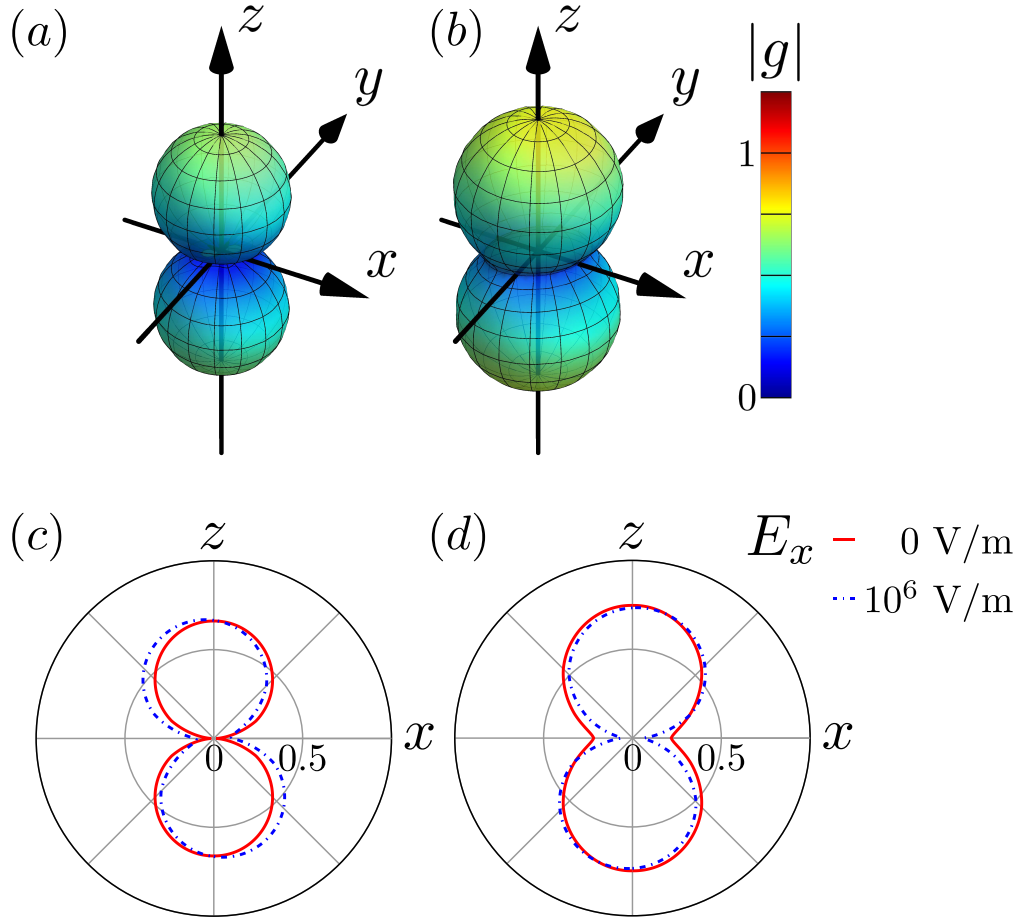
Figure 3.5: $|g_2|$ and $|g_3|$ as functions of the magnetic field direction for $|\boldsymbol{B}| = 1$ T shown in 3D plots for (a) $n = 2$, (b) $n = 3$, and cuts along the xz plane for (c) $n = 2$ and (d) $n = 3$ with electric field $\boldsymbol{E} = (E_x, 0, 0)$.
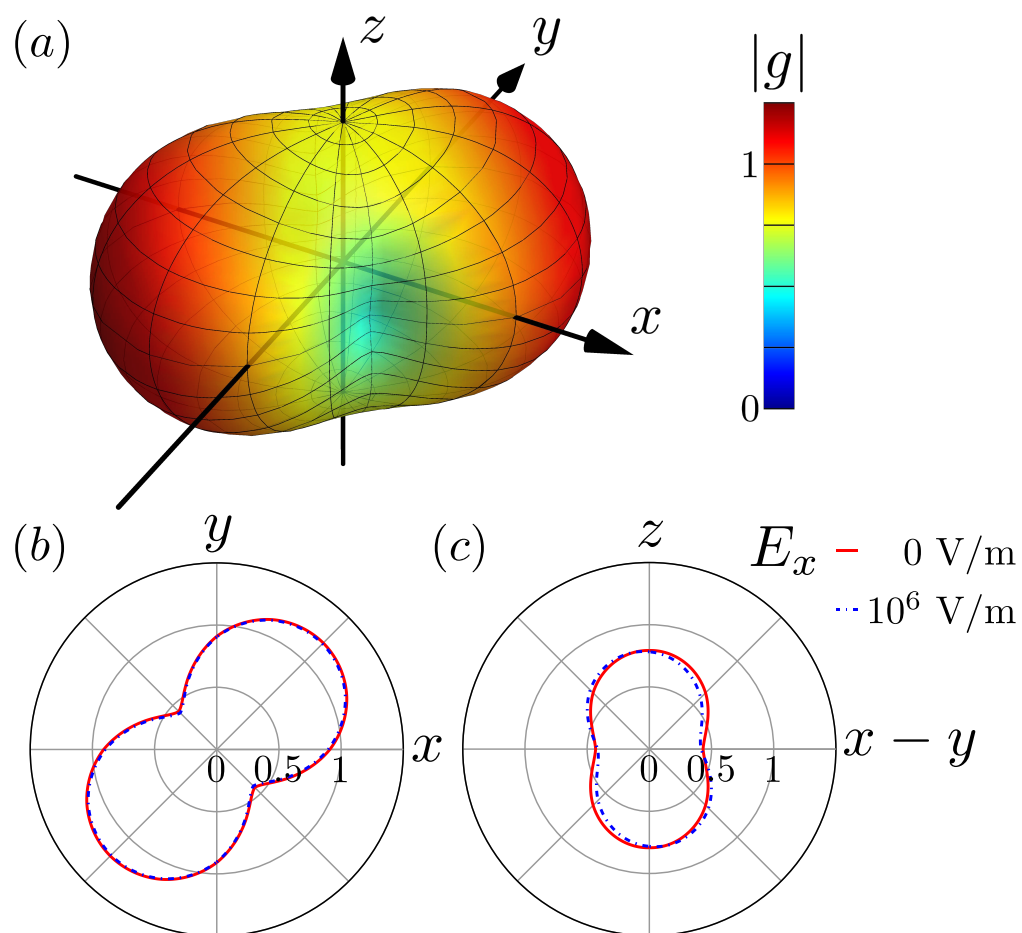
Figure 3.6: $|g_4|$ as a function of the magnetic field direction for $|\boldsymbol{B}| = 1\,\mathrm{T}$ shown in (a) 3D plot, and cuts along the planes (b) xy, and (c) $(x-y)z$ with electric field $\boldsymbol{E} = (E_x, 0, 0)$.
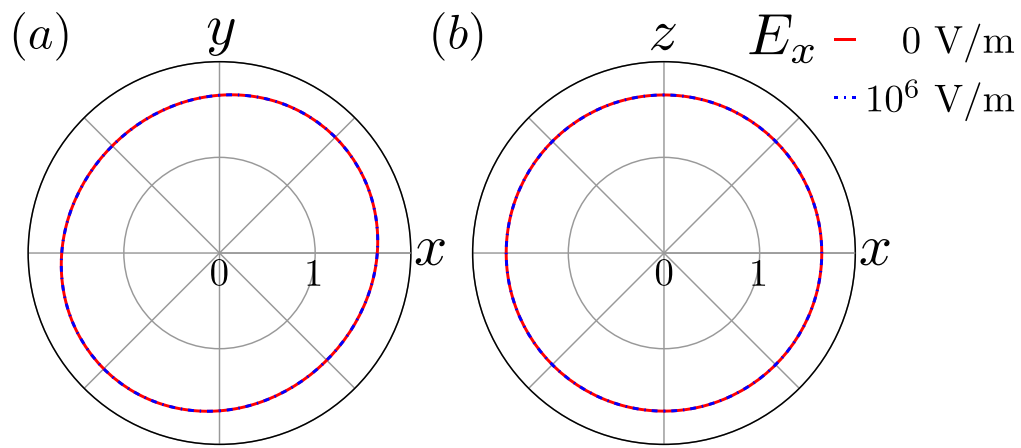
Figure 3.7: $|g_5|$ as a function of the magnetic field direction shown for $|\boldsymbol{B}| = 1$ T in cuts along the planes (a) xy, and (b) xz with electric field $\boldsymbol{E} = (E_x, 0, 0)$. Here we omit the 3D plot since the g factor shows a spherical distribution, where such a plot does not yield further insight.
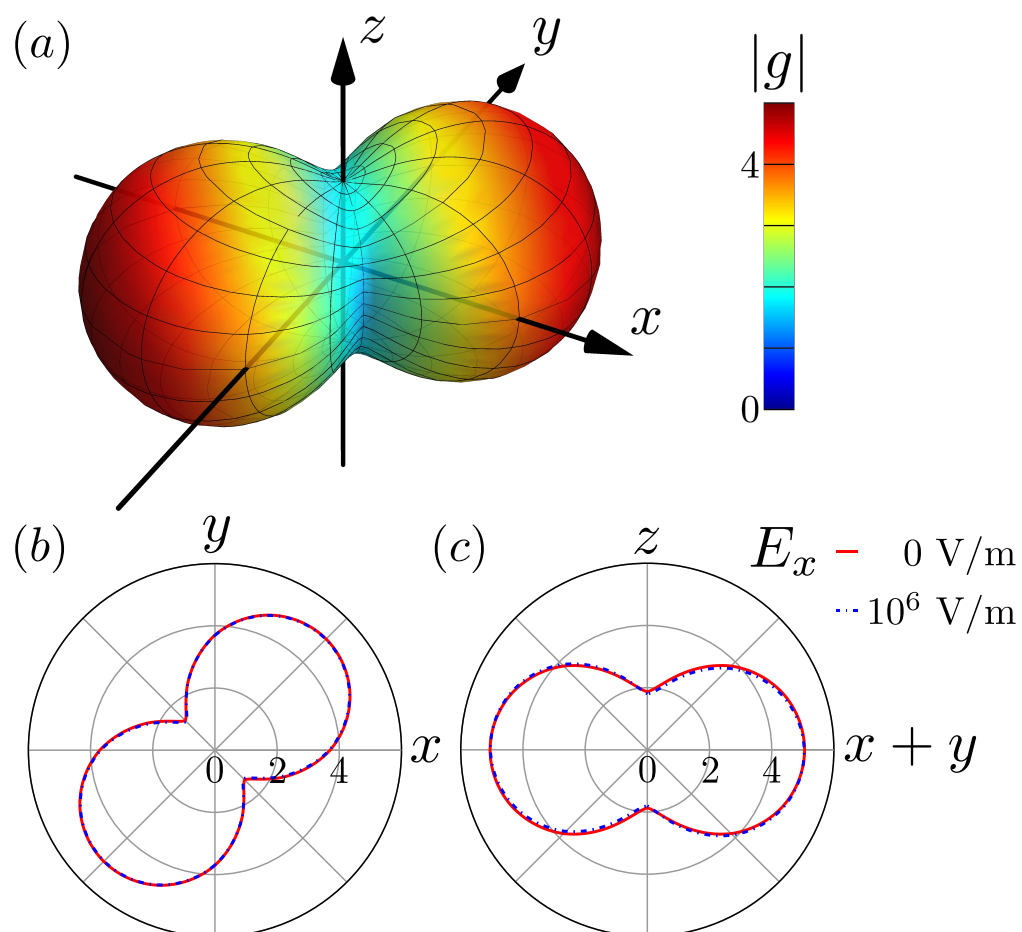
Figure 3.8: $|g_6|$ as a function of the magnetic field direction for $|\boldsymbol{B}| = 1$ T shown in (a) 3D plot, and cuts along the planes (b) xy and (c) $(x+y)z$ with electric field $\boldsymbol{E} = (E_x, 0, 0)$. Note that the color scale changed because $|g_6|$ reaches larger values than the $|g_n|$ of the QD levels with $n < 6$.

Appendix

Trial wave functions

Particle in an isosceles triangle

The Schrödinger equation of a particle confined to a square with sides of length a,

$$-\frac{\hbar^2}{2m_0}\left(\frac{d^2}{dx^2}+\frac{d^2}{dy^2}\right)\psi^\square(x,y)=E^\square\,\psi^\square(x,y),\qquad(A.1)$$

with boundary conditions $\psi^\square(x,y)=0$ for $x=0$, $y=0$, $x=a$ or $y=a$, has the well-known solution

$$\psi^\square_{mn}(x,y)=\frac{2}{a}\,\sin\left(\frac{m\pi}{a}x\right)\,\sin\left(\frac{n\pi}{a}y\right),\qquad(A.2)$$

$$E^\square_{mn}=\frac{\hbar^2\pi^2}{2m_0a^2}\,\left(m^2+n^2\right).\qquad(A.3)$$

The wave function of a particle confined in an isosceles triangle obtained by cutting the square along the diagonal, $\psi^\triangle(x,y)$, is constructed by symmetric and asymmetric linear combination of degenerate solutions to the square problem, $\psi^\square_{mn}$ and $\psi^\square_{nm}$ [Li84], and we find

$$\psi^{\triangle s}_{mn}=\tfrac{1}{\sqrt{2}}\left(\psi^\square_{mn}+\psi^\square_{nm}\right),\qquad(A.4)$$

$$\psi^{\triangle a}_{mn}=\tfrac{1}{\sqrt{2}}\left(\psi^\square_{mn}-\psi^\square_{nm}\right),\qquad(A.5)$$

where $\psi^{\triangle s}_{mn}$ ($\psi^{\triangle a}_{mn}$) vanishes at $x+y=a$ for $m+n$ odd (even). The general wave function takes the form

$$\psi^\triangle_{mn}=\frac{1}{\sqrt{2}}\left(\psi^\square_{mn}+(-1)^{m+n+1}\psi^\square_{nm}\right),\qquad(A.6)$$
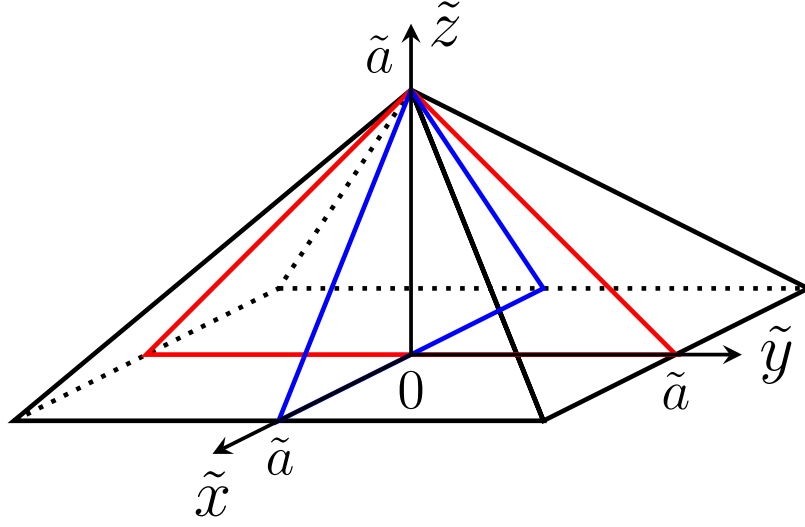
Figure A.1: We span the pyramid volume by multiplying two upright isosceles triangles (red and blue). Note that $\tilde{r}$ and $\tilde{a}$ correspond to r and a in the main text, respectively.

with $m, n = 1, 2, 3, \ldots$ and $m \neq n$ to prevent the construction of a vanishing wave function $\psi^{\triangle}_{mm} = 0$. We apply a coordinate transformation characterized by $x = -[\tilde{x} + (\tilde{y} - \tilde{a})]/2\sqrt{2}$ and $y = [\tilde{x} - (\tilde{y} - \tilde{a})]/2\sqrt{2}$ in order to bring the triangle into upright position, i.e., the apex of the triangle is centered above the base, and find

$$\psi^{\triangle}_{mn}(\tilde{x}, \tilde{y}) = -\psi^{\triangle}_{mn}\left(\tfrac{\tilde{x}+(\tilde{y}-\tilde{a})}{2\sqrt{2}}, \tfrac{\tilde{x}-(\tilde{y}-\tilde{a})}{2\sqrt{2}}\right) \tag{A.7}$$

with $m, n = 1, 2, 3, \ldots, m \neq n$, and $\tilde{a} = a/\sqrt{2}$.

Particle in a square pyramid

Starting from the solution to the two dimensional Schrödinger equation, we construct an ansatz or trial wave function that is not an eigenfunction of the three dimensional (3D) Schrödinger equation but nonetheless fulfills the boundary conditions of the pyramid and expected symmetries. We span the 3D volume of the pyramid with the product of two upright triangles, see Fig. A.1, and find the wave function

$$\psi_{\boldsymbol{m}}(\tilde{\boldsymbol{r}}) = c\,\psi^{\triangle}_{m_x m_z}(\tilde{x}, \tilde{z})\,\psi^{\triangle}_{m_y m_z}(\tilde{y}, \tilde{z})$$

$$= c\prod_{\xi = \tilde{x}, \tilde{y}}\Big[\sin\big(\alpha_\xi\,\xi^+\big)\sin\big(\alpha_z\,\xi^-\big)$$

$$- (-1)^{m_\xi + m_z}\sin\big(\alpha_z\,\xi^+\big)\sin\big(\alpha_\xi\,\xi^-\big)\Big], \tag{A.8}$$

with $\tilde{\boldsymbol{r}} = (\tilde{x}, \tilde{y}, \tilde{z})$, $c = \csc(\pi\tilde{z})/N_{\boldsymbol{m}}$, $\alpha_i = m_i\pi/\tilde{a}$, $m_i = 1, 2, 3, \dots$, $m_x \neq m_z$, $m_y \neq m_z$, $\boldsymbol{m} = (m_x, m_y, m_z)$, $\xi^\pm = \xi \pm (\tilde{z} - \tilde{a})/2$, and $N_{\boldsymbol{m}}$ such that the integral over the pyramid volume yields $\int d^3\tilde{r}\,|\psi_{\boldsymbol{m}}(\tilde{\boldsymbol{r}})|^2 \equiv 1$. Note that we have added the term $\csc(\pi\tilde{z})$ in order to restore the asymptotes at the apex and the base to the correct power law behavior in z that were altered by taking the product $\psi^{\triangle}_{m_x m_z}\psi^{\triangle}_{m_y m_z}$. This factor is essential for obtaining s- and p-wave like states. The energies of state $\psi_{\boldsymbol{m}}$ are given by

$$E_{\boldsymbol{m}} = \frac{\hbar^2}{2m_0}\,\langle\psi_{\boldsymbol{m}}(\tilde{\boldsymbol{r}})|\,(-i\nabla)^2\,|\psi_{\boldsymbol{m}}(\tilde{\boldsymbol{r}})\rangle\,. \tag{A.9}$$

For notational simplicity we use $\psi_{\boldsymbol{m}} \equiv \psi_{m_x m_y m_z}$. We note that the states $\psi_{m_x m_x m_z}$ and $\psi_{m_z m_z m_x}$ coincide by construction and that $\psi_{m_x m_y m_z}$ and $\psi_{m_y m_x m_z}$ are degenerate.

As mentioned above, $\psi_{\boldsymbol{m}}$ is not an eigenfunction of the 3D Schrödinger equation. However, the boundary conditions are fulfilled. In addition, the energies $E_{\boldsymbol{m}}$ are smaller than the eigenenergies of known analytical solutions provided that the correct boundary conditions at the base of the pyramid are taken into account [HRV+12]. Furthermore, the set of eigenfunctions reported in Ref. [HRV+12] is incomplete and in particular lacks the ground state and states with a non-vanishing particle density (of s-wave type) at the center of the pyramid. In contrast, our trial wave functions form a complete set including states with s- and p-wave character. Despite the fact that $\psi_{\boldsymbol{m}}$ is not an eigenfunction, we conclude that our trial wave functions provide a good starting point for analytical investigations of pyramidal quantum dots.

Material parameters

Notation and values

We choose the notation for the parameters exactly as given in Ref. [Win03]. See Table B.1. Due to lack of experimentally validated InAs parameters D', we use InSb values which are assumed to be close to InAs values.

Table B.1: Material parameters used in this work. If not stated otherwise, the parameters were taken from Ref. [Win03].

E_g	[eV]	0.418	
Δ_0	[eV]	0.380	
P	[eVÅ]	9.197	
C_k	[eVÅ]	-0.0112	
m^*	$[m_0]$	0.0229	
g^*		-14.9	
γ_1		20.40	
γ_2		8.30	
γ_3		9.10	
B_{8v}^+	[eVÅ^2]	-3.393	
B_{8v}^-	[eVÅ^2]	-0.09511	
B_{7v}	[eVÅ^2]	-3.178	
κ		7.60	
q		0.39	
C_1	[eV]	-5.08	[Win03, VMRM01]
D_d	[eV]	1	[Win03, VMRM01]
D_u	[eV]	2.7	

D'_u	[eV]	3.18	
C_2	[eV]	1.8	[BP62, VMRM01]
D'		-2	[TWPH88, WAL78]
C_4	[eVÅ]	11.3	[RTRP79, SBGO92]
C_5	[eVÅ]	103.3	[RTRP79, SBGO92]
C'_5	[eVÅ]	76.9	[TRR79]
a_{InAs}	[nm]	6.0583	
a_{GaAs}	[nm]	5.65325	
ν_{InAs}		0.35	[LRS96]

Bibliography

[ADB+06]   M. Atatüre, J. Dreiser, A. Badolato, A. Högele, K. Karrai, and A. Imamoglu, Science **312**, 551 (2006).

[AN92]   D. V. Averin and Y. V. Nazarov, in *Single Charge Tunneling*, edited by H. Grabert and M. H. Devoret, Vol. 294 of NATO ASI Series B: Physics (Plenum, New York, 1992).

[BHH+01]   M. Bayer, P. Hawrylak, K. Hinzer, S. Fafard, M. Korkusinski, Z. R. Wasilewski, O. Stern, and A. Forchel, Science **291**, 451 (2001).

[BKF+99]   M. Bayer, A. Kuther, A. Forchel, A. Gorbunov, V. B. Timofeev, F. Schäfer, J. P. Reithmaier, T. L. Reinecke, and S. N. Walck, Phys. Rev. Lett. **82**, 1748 (1999).

[BN08]   W. Bishara and C. Nayak, Phys. Rev. B **77**, 165302 (2008).

[BP62]   G. L. Bir and G. E. Pikus, Sov. Phys.-Sol. State **3**, 2221 (1962).

[BPC+13]   A. J. Bennett, M. A. Pooley, Y. Cao, N. Sköld, I. Farrer, D. A. Ritchie, and A. J. Shields, Nat. Commun. **4**, 1522 (2013).

[BZBS09]   M. Baraban, G. Zikos, N. Bonesteel, and S. H. Simon, Phys. Rev. Lett. **103**, 076801 (2009).

[CFB+11]   M. Carrega, D. Ferraro, A. Braggio, N. Magnoli, and M. Sassetti, Phys. Rev. Lett. **107**, 146404 (2011).

[CFB+12]   M. Carrega, D. Ferraro, A. Braggio, N. Magnoli, and M. Sassetti, New J. Phys. **14**, 023017 (2012).

[CL08]   S. Chesi and D. Loss, Phys. Rev. Lett. **101**, 146803 (2008).

[CTDL77]   C. Cohen-Tannoudji, B. Diu, and F. Laloe, *Quantum mechanics. Vol. 1*, Wiley, New York, 1977.

[D13]   'Democritus', Encyclopaedia Britannica Online Academic Edition, Encyclopaedia Britannica Inc., retrieved 11 Nov. 2013.

[dCCFK⁺97]   C. de C. Chamon, D. E. Freed, S. A. Kivelson, S. L. Sondhi, and X. G. Wen, Phys. Rev. B **55**, 2331 (1997).

[dFB⁺13]   S. d'Hollosy, G. Fábián, A. Baumgartner, J. Nygård, and C. Schönenberger, arXiv:1309.0726 (2013).

[DHU⁺08]   M. Dolev, M. Heiblum, V. Umansky, A. Stern, and D. Mahalu, Nature **452**, 829 (2008).

[DKT⁺11]   R. S. Deacon, Y. Kanai, S. Takahashi, A. Oiwa, K. Yoshida, K. Shibata, K. Hirakawa, Y. Tokura, and S. Tarucha, Phys. Rev. B **84**, 041302 (2011).

[DP07]   A. De and C. E. Pryor, Phys. Rev. B **76**, 155321 (2007).

[FD87]   T. A. Fulton and G. J. Dolan, Phys. Rev. Lett. **59**, 109 (1987).

[FFN06]   P. Fendley, M. P. A. Fisher, and C. Nayak, Phys. Rev. Lett. **97**, 036801 (2006).

[FFN07]   P. Fendley, M. P. A. Fisher, and C. Nayak, Phys. Rev. B **75**, 045317 (2007).

[FGK⁺07]   D. E. Feldman, Y. Gefen, A. Kitaev, K. T. Law, and A. Stern, Phys. Rev. B **76**, 085333 (2007).

[FK06]   D. E. Feldman and A. Kitaev, Phys. Rev. Lett. **97**, 186803 (2006).

[FMAE⁺07]   J. Fabian, A. Matos-Abiague, C. Ertler, P. Stano, and I. Žutić, Acta Phys. Slov. **57**, 565 (2007).

[FNTW98]   E. Fradkin, C. Nayak, A. Tsvelik, and F. Wilczek, Nucl. Phys. B **516**, 704 (1998).

[FRNDS08]   A. E. Feiguin, E. Rezayi, C. Nayak, and S. Das Sarma, Phys. Rev. Lett. **100**, 166803 (2008).

[FRY⁺09]   A. E. Feiguin, E. Rezayi, K. Yang, C. Nayak, and S. Das Sarma, Phys. Rev. B **79**, 115322 (2009).

[GCL⁺95]   M. Grundmann, J. Christen, N. N. Ledentsov, J. Böhrer, D. Bimberg, S. S. Ruvimov, P. Werner, U. Richter, U. Gösele, J. Heydenreich, V. M. Ustinov, A. Y. Egorov, A. E. Zhukov, P. S. Kop'ev, and Z. I. Alferov, Phys. Rev. Lett. **74**, 4043 (1995).

[Gia04]   T. Giamarchi, *Quantum Physics in One Dimension*, Oxford University Press, USA, 2004.

[GL97]   M. R. Geller and D. Loss, Phys. Rev. B **56**, 9692 (1997).

[GL04]   V. N. Golovach and D. Loss, Phys. Rev. B **69**, 245327 (2004).

[GNT04]   A. O. Gogolin, A. A. Nersesyan, and A. M. Tsvelik, *Bosonization and strongly correlated systems*, Cambridge University Press, 2004.

[Goe05]   J. W. v. Goethe, *Faust*, The World Publishing Company, Cleveland, Ohio and New York, N.Y., 2005.

[GSB95]   M. Grundmann, O. Stier, and D. Bimberg, Phys. Rev. B **52**, 11969 (1995).

[HKP⁺07]   R. Hanson, L. P. Kouwenhoven, J. R. Petta, S. Tarucha, and L. M. K. Vandersypen, Rev. Mod. Phys. **79**, 1217 (2007).

[HRV⁺12]   P. P. Horley, P. Ribeiro, V. R. Vieira, J. González-Hernández, Y. V. Vorobiev, and L. G. Trápaga-Martínez, Physica E **44**, 1602 (2012).

[Ihn10]   T. Ihn, *Semiconductor Nanostructures, Quantum States and Electronic Transport*, Oxford University Press, Oxford; New York, 2010.

[Jai07]   J. K. Jain, *Composite Fermions*, Cambridge University Press, Cambridge, 2007.

[JCS⁺03]   Y. Ji, Y. Chung, D. Sprinzak, M. Heiblum, D. Mahalu, and H. Shtrikman, Nature **422**, 415 (2003).

[JMSS12]   P.-Q. Jin, M. Marthaler, A. Shnirman, and G. Schön, Phys. Rev. Lett. **108**, 190506 (2012).

[KAT01]   L. P. Kouwenhoven, D. G. Austing, and S. Tarucha, Rep. Prog. Phys. **64**, 701 (2001).

[KL13]   C. Kloeffel and D. Loss, Annu. Rev. Cond. Mat. Phys. **4**, 51 (2013).

[LD98]   D. Loss and D. P. DiVincenzo, Phys. Rev. A **57**, 120 (1998).

[LFG06]   K. T. Law, D. E. Feldman, and Y. Gefen, Phys. Rev. B **74**, 045319 (2006).

[LHR07]   M. Levin, B. I. Halperin, and B. Rosenow, Phys. Rev. Lett. **99**, 236806 (2007).

[Li84]   W.-K. Li., J. Chem. Educ. **61**, 1034 (1984).

[LRNF07]   S.-S. Lee, S. Ryu, C. Nayak, and M. P. A. Fisher, Phys. Rev. Lett. **99**, 236807 (2007).

[LRS96]   M. E. Levinshtein, S. Rumyantsev, and M. Shur, *Handbook series on semiconductor parameters*, World Scientific, Singapore, 1996.

[LSG$^+$96] N. N. Ledentsov, V. A. Shchukin, M. Grundmann, N. Kirstaedter, J. Böhrer, O. Schmidt, D. Bimberg, V. M. Ustinov, A. Y. Egorov, A. E. Zhukov, P. S. Kopev, S. V. Zaitsev, N. Y. Gordeev, Z. I. Alferov, A. I. Borovkov, A. O. Kosogov, S. S. Ruvimov, P. Werner, U. Gösele, and J. Heydenreich, Phys. Rev. B **54**, 8743 (1996).

[Mor98]   R. H. Morf, Phys. Rev. Lett. **80**, 1505 (1998).

[MR91]   G. Moore and N. Read, Nucl. Phys. B **360**, 362 (1991).

[MRPPM02]   G. Medeiros-Ribeiro, M. V. B. Pinheiro, V. L. Pimentel, and E. Marega, Appl. Phys. Lett. **80**, 4229 (2002).

[MRZ$^+$07] J. B. Miller, I. P. Radu, D. M. Zumbuhl, E. M. Levenson-Falk, M. A. Kastner, C. M. Marcus, L. N. Pfeiffer, and K. W. West, Nat. Phys. **3**, 561 (2007).

[MS08]   G. Möller and S. H. Simon, Phys. Rev. B **77**, 075319 (2008).

[ND10]   A. V. Nenashev and A. V. Dvurechenskii, J. Appl. Phys. **107**, 064322 (2010).

[NSS$^+$08] C. Nayak, S. H. Simon, A. Stern, M. Freedman, and S. Das Sarma, Rev. Mod. Phys. **80**, 1083 (2008).

[PDGM+10] D. Press, K. De Greve, P. L. McMahon, T. D. Ladd, B. Friess, C. Schneider, M. Kamp, S. Höfling, A. Forchel, and Y. Yamamoto, Nat. Photonics **4**, 367 (2010).

[PF06] C. E. Pryor and M. E. Flatté, Phys. Rev. Lett. **96**, 026804 (2006).

[PF07] C. E. Pryor and M. E. Flatté, Phys. Rev. Lett. **99**, 179901 (2007).

[PLZY08] D. Press, T. D. Ladd, B. Zhang, and Y. Yamamoto, Nature **456**, 218 (2008).

[PMS+12] K. D. Petersson, L. W. McFaul, M. D. Schroer, M. Jung, J. M. Taylor, A. A. Houck, and J. R. Petta, Nature **490**, 380 (2012).

[PPF08] J. Pingenot, C. E. Pryor, and M. E. Flatté, Appl. Phys. Lett. **92**, 222502 (2008).

[PPF11] J. Pingenot, C. E. Pryor, and M. E. Flatté, Phys. Rev. B **84**, 195403 (2011).

[PPS97] C. Pryor, M.-E. Pistol, and L. Samuelson, Phys. Rev. B **56**, 10404 (1997).

[Pry98] C. Pryor, Phys. Rev. B **57**, 7190 (1998).

[RG00] N. Read and D. Green, Phys. Rev. B **61**, 10267 (2000).

[RH00] E. H. Rezayi and F. D. M. Haldane, Phys. Rev. Lett. **84**, 4685 (2000).

[RL02] P. Recher and D. Loss, Phys. Rev. B **65**, 165327 (2002).

[RMM+08] I. P. Radu, J. B. Miller, C. M. Marcus, M. A. Kastner, L. N. Pfeiffer, and K. W. West, Science **320**, 899 (2008).

[RR99] N. Read and E. Rezayi, Phys. Rev. B **59**, 8084 (1999).

[RSL00] P. Recher, E. V. Sukhorukov, and D. Loss, Phys. Rev. Lett. **85**, 1962 (2000).

[RTRP79] R. Ranvaud, H. R. Trebin, U. Rössler, and F. H. Pollak, Phys. Rev. B **20**, 701 (1979).

[RWS+95]   S. Ruvimov, P. Werner, K. Scheerschmidt, U. Gösele, J. Hey-
            denreich, U. Richter, N. N. Ledentsov, M. Grundmann,
            D. Bimberg, V. M. Ustinov, A. Y. Egorov, P. S. Kopev, and
            Z. I. Alferov, Phys. Rev. B **51**, 14766 (1995).

[SBGO92]   M. Silver, W. Batty, A. Ghiti, and E. P. O'Reilly, Phys. Rev.
            B **46**, 6781 (1992).

[SBS+99]   C. Schönenberger, A. Bachtold, C. Strunk, J.-P. Salvetat, and
            L. Forró, Appl. Phys. A **69**, 283 (1999).

[SGB99]   O. Stier, M. Grundmann, and D. Bimberg, Phys. Rev. B **59**,
            5688 (1999).

[SJ10]   P. Stano and P. Jacquod, Phys. Rev. B **82**, 125309 (2010).

[SPV+12]   M. Stern, B. A. Piot, Y. Vardi, V. Umansky, P. Plochocka,
            D. K. Maude, and I. Bar-Joseph, Phys. Rev. Lett. **108**, 066810
            (2012).

[TDO+13]   S. Takahashi, R. S. Deacon, A. Oiwa, K. Shibata, K. Hi-
            rakawa, and S. Tarucha, Phys. Rev. B **87**, 161302 (2013).

[TGKM12]   L. Tiemann, G. Gamez, N. Kumada, and K. Muraki, Science
            335, 828 (2012).

[TN01]   M. Taketani and M. Nagasaki, *The formation and logic of
            quantum mechanics.* World Scientific, River Edge, N.J., 2001.

[TRR79]   H. R. Trebin, U. Rössler, and R. Ranvaud, Phys. Rev. B **20**,
            686 (1979).

[TSL12]   F. Troiani, D. Stepanenko, and D. Loss, Phys. Rev. B **86**,
            161409 (2012).

[TWPH88]   H.-R. Trebin, B. Wolfstädter, H. Pascher, and H. Häfele,
            Phys. Rev. B **37**, 10249 (1988).

[vBSK+12]   J. van Bree, A. Y. Silov, P. M. Koenraad, M. E. Flatté, and
            C. E. Pryor, Phys. Rev. B **85**, 165323 (2012).

[VDGS12]   G. Viola, S. Das, E. Grosfeld, and A. Stern, Phys. Rev. Lett.
            109, 146801 (2012).

[VLP$^+$00]   E. E. Vdovin, A. Levin, A. Patan, L. Eaves, P. C. Main, Y. N. Khanin, Y. V. Dubrovskii, M. Henini, and G. Hill, Science **290**, 122 (2000).

[VMRM01]   I. Vurgaftman, J. R. Meyer, and L. R. Ram-Mohan, J. Appl. Phys. **89**, 5815 (2001).

[VTH13]   Y. V. Vorobiev, T. V. Torchynska, and P. P. Horley, Physica E **51**, 42 (2013).

[VYPW11]   V. Venkatachalam, A. Yacoby, L. Pfeiffer, and K. West, Nature **469**, 185 (2011).

[WAL78]   M. H. Weiler, R. L. Aggarwal, and B. Lax, Phys. Rev. B **17**, 3269 (1978).

[Wen90]   X. G. Wen, Phys. Rev. B **41**, 12838 (1990).

[Wen92]   X.-G. Wen, Int. J. Mod. Phys. B **6**, 1711 (1992).

[Wen95]   X.-G. Wen, Adv. Phys. **44**, 405 (1995).

[WF10]   C. Wang and D. E. Feldman, Phys. Rev. B **82**, 165314 (2010).

[WHRY08]   X. Wan, Z.-X. Hu, E. H. Rezayi, and K. Yang, Phys. Rev. B **77**, 165316 (2008).

[Win03]   R. Winkler, *Spin-Orbit Coupling Effects in Two-Dimensional Electron and Hole Systems*, Springer, Berlin, 2003.

[ZHR09]   O. S. Zozulya, M. Haque, and N. Regnault, Phys. Rev. B **79**, 045409 (2009).

Curriculum Vitae

Robert Manfred Zielke

Date of birth: 12 February 1985
Place of birth: Lörrach, Germany

Education

November 2009 - March 2014	*PhD in Theoretical Physics* University of Basel, Switzerland Advisor: Prof. Dr. Daniel Loss
2008 - 2009	*MSc in Physics* University of Basel, Switzerland Advisor: Prof. Dr. Daniel Loss
2005 - 2008	*BSc in Physics* University of Basel, Switzerland
2004 - 2005	*Military Service* Stetten a.k.M. & Todtnau, Germany
1995 - 2004	*Abitur (German highschool diploma)* Lise-Meitner-Gymnasium, Grenzach-Wyhlen, Germany

List of publications

An asterisk denotes a publication covered in this thesis.

*   R. Zielke, F. Maier, and D. Loss, *"Anisotropic g factor in InAs self-assembled quantum dots"*, Phys. Rev. B **89**, 115438 (2014).

*   R. Zielke, B. Braunecker, and D. Loss, *"Cotunneling in the $\nu = 5/2$ fractional quantum Hall regime"*, Phys. Rev. B **86**, 235307 (2012).